

Scuola di Scienze
Dipartimento di Fisica e Astronomia
Corso di Laurea in Fisica

Computational study of resting state network dynamics

Relatore:
Prof. Gastone Castellani

Presentata da:
Daniele Corradini

Sessione II
Anno Accademico 2016/2017

“When we take a general view of the wonderful stream of our consciousness, what strikes us first is the different pace of its parts. Like a bird’s life, it seems to be made of an alternation of flights and perchings.”

William James

Abstract

Lo scopo di questa tesi è quello di mostrare, attraverso una simulazione con il software *The Virtual Brain*, le più importanti proprietà della dinamica cerebrale durante il *resting state*, ovvero quando non si è coinvolti in nessun compito preciso e non si è sottoposti a nessuno stimolo particolare. Si comincia con lo spiegare cos'è il *resting state* attraverso una breve revisione storica della sua scoperta, quindi si passano in rassegna alcuni metodi sperimentali utilizzati nell'analisi dell'attività cerebrale, per poi evidenziare la differenza tra connettività strutturale e funzionale. In seguito, si riassumono brevemente i concetti dei sistemi dinamici, teoria indispensabile per capire un sistema complesso come il cervello. Nel capitolo successivo, attraverso un approccio 'bottom-up', si illustrano sotto il profilo biologico le principali strutture del sistema nervoso, dal neurone alla corteccia cerebrale. Tutto ciò viene spiegato anche dal punto di vista dei sistemi dinamici, illustrando il pionieristico modello di Hodgkin-Huxley e poi il concetto di dinamica di popolazione. Dopo questa prima parte preliminare si entra nel dettaglio della simulazione. Prima di tutto si danno maggiori informazioni sul software *The Virtual Brain*, si definisce il modello di network del *resting state* utilizzato nella simulazione e si descrive il 'connettoma' adoperato. Successivamente vengono mostrati i risultati dell'analisi svolta sui dati ricavati, dai quali si mostra come la criticità e il rumore svolgano un ruolo chiave nell'emergenza di questa attività di fondo del cervello. Questi risultati vengono poi confrontati con le più importanti e recenti ricerche in questo ambito, le quali confermano i risultati del nostro lavoro. Infine, si riportano brevemente le conseguenze che porterebbe in campo medico e clinico una piena comprensione del fenomeno del *resting state* e la possibilità di virtualizzare l'attività cerebrale.

Contents

1	Introduction	1
2	What is ‘resting state’ ?	3
2.1	A brief history	3
2.2	How to investigate the brain	4
2.3	Structural vs Functional Connectivity	7
3	Dynamical systems in Neuroscience	9
3.1	Basic notions of Dynamical Systems	9
3.2	Equilibria classification and attractors	10
3.3	Bifurcations	15
4	From neurobiology to dynamical models	19
4.1	The Neurons	19
4.2	Neuron dynamics	23
4.3	The Brain	30
4.4	Population dynamics	31
5	Materials and Methods	37
5.1	The Virtual Brain	37
5.2	The Resting State Network model	38
5.3	Simulation Set-up	41
6	Results and discussion	43
6.1	Analysis results	43
6.2	Comparison with the literature	47
6.3	Clinical Applications	50
7	Conclusion	53
	Bibliography	55

Chapter 1

Introduction

It has been appreciated for at least two millennia that the brains of humans exhibit ongoing activity regardless of the presence or absence of any observable behaviours. As noted by Seneca in 60 A.D., *“The fact that the body is lying down is no reason for supposing that the mind is at peace. Rest is... far from restful”* (Seneca, 1969). Given the apparently contradictory characterization of “rest” it is prudent to begin with a definition. In the context of experimentation, “rest” is an operational definition referring to a constant condition without imposed stimuli or other behaviourally salient events [13]. However, interest in the interplay between the intrinsic activity of the brain and the external world has seen a revival over the past decade, especially in neuroimaging. In fact, an assumption in many of the early studies was that such intrinsic brain activity is irrelevant and sufficiently random that it averages out in statistical analysis. However, despite the most elegant experimental designs, there were consistent patterns of deactivation that often accompanied increased cognitive demands. Hence, several researchers began to examine these deactivations based on the idea that the low-level baseline tasks were active states and that the patterns of activation and deactivation represented a shift in the balance from a focus on the internal state of the subject and its ruminations, to one on the external environment [15]. Numerous experimental investigations have shown that spontaneous brain activity during rest is highly structured into characteristic spatio-temporal patterns, the so-called resting-state networks (RSNs). The observation that there are relatively consistent distributed patterns of activity during rest led to the suggestion that it might be possible to characterize network dynamics without needing an explicit task to drive brain activity. This possibility has been explored in studies of RSNs in functional magnetic resonance imaging (fMRI). It has been seen that RSNs reflect the anatomical connectivity between brain areas in a network but cannot be understood in those terms alone. The missing link for understanding the formation and dissolution of RSNs is the dynamics, so in order to understand this emergent features we need theoretical models that allowed us to study the relation between anatomical structure and RSN [17]. Many theories suggest possible tasks of the brain at rest. A sceptical view is to think it is just due to experimental noise, such as heart-beat, respiration, and so forth. Many evidences, however, suggest this is not the case, and many preprocessing steps have to be carried out in order to rule out these contributions. More optimistic and fascinating theories involve processing of previously acquired information, memory consolidation and preparation to a future task. Unconstrained cognition alone does not account for the greatest part of intrinsic activity although it undoubtedly contributes a small increment. The principal reasons for this assertion may be stated as follows:

- Imposed tasks evoke responses that are modest in magnitude in comparison to intrinsic activity. This is why averaging is required to extract meaningful

responses from the ongoing background. There is no reason to suppose that unconstrained thoughts are more energy demanding than constrained ones.

- Resting state activity persists, albeit in modified form, during slow wave sleep and even during surgical anaesthesia, states in which cognition generally is assumed to be absent or at least very attenuated.

Hence, something other than unconstrained cognition must be posited to account for most intrinsic activity [13]. A definitive answer, however, is far from being reached, and a lot of work has to be done even to understand much simpler processes.

The goal of this thesis is to analyse a simple brain model which describes the resting state network dynamics and shows that their working point is at the edge of the instability. Like in many complex biological system, also in the brain criticality has a pivotal role (see Fig. 1.1). Moreover, we will see also that the ongoing cerebral activity have useful clinical applications. Before describes the materials and methods used for this thesis, it is introduced a brief framework concerning the concept of resting state and the brain modelling. This introductory chapters outlines the neuroscientific framework of the study and they are certainly helpful for understanding the presented work.

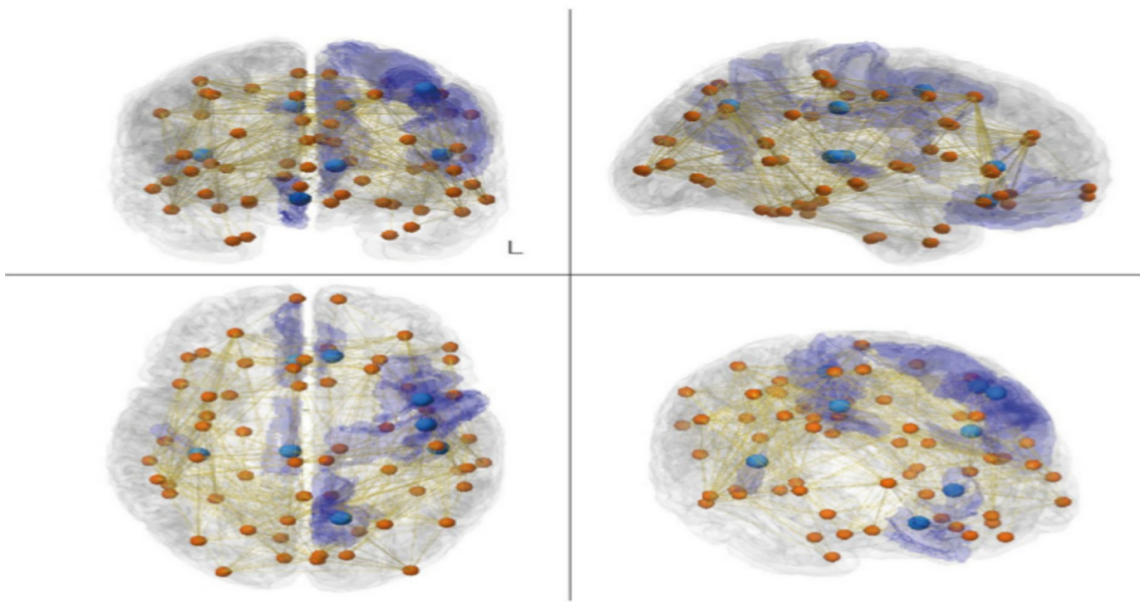


FIGURE 1.1: The figure shows the dynamical core regions on the edge of bifurcation (location of neural masses shown in light blue and transparent blue for the full region). These are the nodes with the ability to react immediately to changes in the predicted input and thus likely to drive the rest of the brain networks. The eight regions are clearly lateralised; and in the right hemisphere encompass medial orbitofrontal cortex, posterior cingulate cortex and transverse temporal gyrus, while in the left hemisphere include caudal middle frontal gyrus, precentral gyrus, precuneus cortex, rostral anterior cingulate cortex and transverse temporal gyrus. Interestingly, some of these regions are part of the default mode network while others have been implicated in memory processing, auditory processing, selection for action and motor execution [8].

Chapter 2

What is 'resting state' ?

The resting state is the spontaneous state of the brain, i.e. the activity of the brain in absence of any external stimuli or other behaviourally salient events, when we are supposedly not doing anything. Unlike the equilibrium state of an unperturbed noisy physical system, the spontaneous state of the brain does not show a trivial random activity, as was expected by the scientists until two decades ago. The underlying anatomical structure alone does not explain all the coordinated activity taking place in the brain even in absence of any specific externally-driven task, so we will see that structural and functional connectivity are related but they also have specific origins and features.

In this first chapter we provide a general overview of the resting state, following its history and research development during the last decades; then we highlight the different neuroimaging techniques used in resting state study, in particular we focus on the functional MRI. At the end there will be a current discussion on the difference between anatomical structure and effective functional neuronal activity.

2.1 A brief history

Below we present a brief account of scientific milestones that have shaped our view of the resting state.

The first scientist to explicitly address the significance of patterned nervous activity may have been Thomas Henry Huxley, in his book on the crayfish (1879), where he emphasized the extent to which the crayfish exhibits highly organized behaviours in response to the simplest stimuli. In 1933, George Bishop observed cyclic changes of excitability in the visual cortex of the rabbit during stimulation of the optic nerve and he clearly understood that the brain's response to stimuli is modulated by fluctuating endogenous activity. More recent, fMRI-based examples of this principle include the demonstration that percepts as well as actions are modulated by ongoing activity. These experiments are grounded in the view, articulated in the early part of the 20th century by the physiologist T. Graham Brown, that the brain's operations are mainly intrinsic, involving acquisition and maintenance of information for interpreting, responding to and even predicting environmental demands. In 1996, Lawrence R. Pinneo forcefully argued that ongoing neural activity is essential to brain function. Pinneo related tonic neural activity to arousal and suggested that this activity is what enables the brain to efficiently respond to environmental events. These ideas antedate by at least 25 years similar notions that today are discussed under the heading of stochastic resonance. In 1929, Hans Berger reported the first human EEG recordings. Berger understood that the EEG was related to mental activity which adds only a small increment to the cortical work which is going on continuously and not only in the waking state. Response averaging enabled researchers to extract reproducible

waveforms from the ongoing EEG and relate these responses to controlled stimuli. This basic paradigm was carried forward as new techniques for acquiring physiological data became available, e.g., single unit recording, optical imaging and ultimately, fMRI. Until recently, the preponderance of neuroscience research has been conducted by averaging away anything not phase synchronous with events of interest. However, the view that all that background activity was just noise changed and the researchers started to take in account the intrinsic neuronal activity, convinced also by the brain metabolic investigation. In 1948, Sokoloff and his colleagues noted that, while the human brain is only 2% of the body weight, it accounts for 20% of the body's energy consumption, ten times the amount expected on a per weight basis. These measurements were, of course, made in the resting state. In 1955, the same group had normal subjects perform a difficult mental arithmetic task while whole-brain blood flow and oxygen consumption were measured. When these measurements were compared with the resting state in the same subjects, no change in either whole-brain blood flow or oxygen consumption was observed. Thoughtfully considered, these data present a challenge to those wishing to study brain function when it is realized that most of the brain's activity is intrinsic. Therefore, some began to include a resting state in their imaging studies and the results of doing so were surprising and most interesting. These appeared as activity decreases from a resting state during the performance of goal-directed tasks. These studies generated iconic images of a constellation of brain regions now generally referred to as the default mode network or DMN. It is currently widely accepted that a specific set of brain areas decreases activity during performance of a remarkably wide range of tasks as compared to a control condition. The observation of task-induced activity decreases exhibiting a stereotypical topography was surprising because the involved areas had not previously been recognized as a functional system in the same sense as the motor or visual systems. Compelling evidence of a DMN equivalent has been demonstrated in the monkey and suggestive evidence has been found in the cat and mouse. It is important to note that the DMN is not unique in exhibiting both high levels of baseline metabolism and organized functional activity in the resting state. These are properties of all cortical functional systems and their subcortical connections. It had been known since the advent of fMRI that the BOLD signal exhibits slow spontaneous fluctuations although this phenomenon was initially regarded as noise. However, that these fluctuations are of neural origin was not established until Bharat Biswal and colleagues, in 1995, demonstrated that resting state BOLD signals are temporally correlated within the somatomotor system. The neuroscience community, with few exceptions, was remarkably slow to take note of this important result. The significance of resting state BOLD signal correlations was brought forcefully to our attention when Michael Greicius and colleagues generated an image of the DMN using a seed region of interest in the posterior cingulate cortex [13].

2.2 How to investigate the brain

There are different methods to investigate the structure as well as the function of the brain. The techniques mainly divide into two distinct classes: electro-physiological recording and functional imaging. The formers directly detect neural activity and below we briefly describe the most common techniques are electroencephalography (EEG), electrocorticography or internal EEG (ECoG, or iEEG), magneto-encephalography (MEG) and multielectroarray recording (MEA).

- EEG is a non-invasive technique, because the electrodes are placed along the scalp. While having a high temporal resolution, it has really poor spatial resolution. It is mainly used to detect overall increase in brain activity such in epilepsy, or in behavioural studies.
- When EEG is performed with intracranial electrodes it is called electrocorticography (ECoG), or intracranial electroencephalography (iEEG). Here electrodes are placed directly on the exposed surface of the brain. Since it involves a craniotomy (a surgical incision into the skull) to implant the electrode grid, ECoG is an invasive procedure and it is not applied on healthy brains, thus it is used when surgery is required for other purposes.
- MEG is the analogous of EEG which detects magnetic fields produced by electrical currents occurring naturally in the brain, rather than electric signals. Arrays of superconducting devices are used as magnetometer. MEG, as EEG, applies on basic research into perceptual and cognitive brain processes, localising regions affected by pathology before surgical removal, and determining the function of various parts of the brain.
- Multielectrode arrays (MEAs) or microelectrode arrays are devices containing multiple plates through which neural signals are obtained or delivered. These plates serve as neural interfaces that connect neurons to electronic circuitry. MEAs can be implantable or non-implantable, used in vivo or in vitro, respectively.

On the other hand, imaging techniques are mainly PET (Positron Emission Tomography) and fMRI (functional Magnetic Resonance Imaging).

- PET is a nuclear medicine technique used to observe metabolic processes in the body. After the injection of a radionuclide tracer, the system detects the pairs of gamma emitted by the positrons. The tracer is introduced in the body through a biologically active molecule, for example Fluorodeoxyglucose (FDG). Fluorodeoxyglucose is uptaken by the brain when needed and thus in these areas pairs of gamma rays are produced. This is useful in exploring the presence of cancer metastasis. The drawback of this technique is that, even though not directly invasive, the injection of a radioisotope is harmful for the organism.
- fMRI is a non-invasive technique which does not directly measure the activity, but relies on the oxygen consumption in areas where energy is required, measuring the Blood Oxygen Level Dependent (BOLD) signal.

As the last technique is the mainly used to reveal the manifestation of spontaneous neuronal activity it will be described more in detail. fMRI has a much better spatial resolution than electrophysiology recordings (about 3 mm) which goes to the detriment of temporal resolution (about 2 seconds, whereas EEG can reach 0.01 seconds). Moreover, fMRI detects well signal coming from inner areas, whereas EEG detects better superficial signals, given that electrodes are placed on the scalp. Studies utilising PET and EEG recordings are consistent with data obtained from fMRI and thus provide a proof of the validity of fMRI as a technique to study brain networks.

Physical principles of fMRI rely on the magnetic property of materials, in particular materials whose constituent nuclei have non-zero spin. Since spin has a magnetic moment associated with it, when these nuclei are placed in a magnetic field B_0 , they align themselves with the magnetic field, distributing in the possible energy levels according to the Boltzmann distribution. As a result a total magnetisation vector \vec{M}

is again aligned with the total magnetic field. When the nuclei placed in such magnetic field are also subjected to a time-varying (radio-frequency) electromagnetic pulse $\vec{B}_1(t)$, perpendicular to \vec{B}_0 , the magnetisation varies. MR images are related to how the system goes back to the equilibrium state. There are two characteristic times which guide this relaxation, usually called T_1 and T_2 . The first refers to the spin-lattice relaxation when recovering M_z , namely how fast the magnetic moments realign with \vec{B}_0 , the second refers to spin-spin interaction and depends on the different chemical neighbourhood in which the nuclei are placed. A universal feature is that $T_2 < T_1$. The two equations representing the evolution of the magnetisation along time are called Bloch equations and lead to

$$M_z(t) = M_z(0)e^{-t/T_1} + M_0(1 - e^{-t/T_1}) \quad (2.1)$$

and to

$$M_{xy}(t) = M_{xy}(0)e^{-t/T_2} \quad (2.2)$$

for the components which are parallel and perpendicular to \vec{B}_0 , respectively. Since the decay of the signal following a single radio-frequency pulse is usually too fast and depends mainly on field inhomogeneities, sequences of impulses are used. Combining (2.1) and (2.2), after some manipulations one gets the following equation for a particular sequence, known as spin-echo, with so called the spin-warp method:

$$M_{xy}(T_R, T_E) = M_0[1 - e^{-T_R/T_1}(2e^{T_E/2T_1} - 1)]e^{-T_E/T_2} \quad (2.3)$$

Here T_R and T_E are two different parameters used in the sequence. In particular T_R is the aforementioned repetition time, whereas T_E is called echo time. From (2.3) one can see that modifying the parameters T_E and T_R , one can weight the image in T_1 or T_2 . This means that if different tissues or areas have different decay times, these parameters are chosen in a way that the signal from one tissue or area has completely decayed, while the other is still present. Structural images are T1-weighted: white matter (more fatty) has a signal decreasing faster than grey matter, in that its relaxation time is smaller, while for functional images a T2 weighting is often employed. Let us examine the brain energy metabolism characteristics that lead to the BOLD signal formation. The activation of a brain region requires energy in form of oxygen (O_2) and glucose, transported by blood flows, which will be transformed in ATP. The hemoglobin molecule (Hb) is able to transport four O_2 molecules. In fact, the Hb molecule is composed by 4 units; at the center of each unit there is a Fe atom, which is responsible of the link with the O_2 . The link or the separation between O_2 and Hb produces a change in the magnetic nature of the hemoglobin molecule. When Hb is not linked to O_2 (deoxyhemoglobin) the 4 Fe atoms are in the higher spin state ($S = 2$); consequently, Hb molecules are attracted by any externally applied magnetic field: Hb is paramagnetic. On the other hand, when O_2 is bound to Hb (oxyhemoglobin, HbO_2) the two electrons are paired and, consequently, they are in the state of lower energy with Fe spin state $S=0$: now the HbO_2 is diamagnetic. Since the deoxyhemoglobin is paramagnetic, it is able to reduce the NMR signal in the images weighted in T_2 ; indeed, the rate of loss of proton spin phase coherence, measured through T_2 , can be modulated by the presence of intravoxel deoxyhaemoglobin. Instead, the oxyhemoglobin, which is diamagnetic, does not modify the NMR signal. During the neural activation of a brain area, there is an higher incoming blood flux with respect to the blood incoming flux during rest; in such area blood vessels expand and the brought-in oxygen is more than the oxygen consumed in burning glucose. Therefore, although paradoxical, in the activate

brain region the concentration of oxygenated blood increases, and the concentration of deoxygenated blood decreases respect to the neighbour region, non-active, brain areas.

2.3 Structural vs Functional Connectivity

There are different ways of studying connections in the brain, each of which reflects different nature of connections: structural, functional and effective connectivity:

- The first, as the name says, reflects the anatomical links that are present among brain regions, mainly represented by axon fibers.
- The second represents co-activation patterns, that is it associates regions whose signals are related, independently of physical links; it is often measured through correlation or spectral coherence.
- The third, inspects also the causality of this relation, with methods such as perturbation of the system and the study of its time series through the use of Granger Causality and transfer entropy.

In this thesis we will considerer mainly the first two type of connectivity.

In more recent times, the preferred approach moves its steps from the notion of functional connectivity: the temporal correlation in the recorded BOLD activity using fMRI data. In practice, the resting state a_{ij} Functional Connectivity (FC) is a matrix whose each entry is the correlation (generally the Pearson correlation) in time between the intrinsic activity of the neural source i and the neural source j . A meaningful finding is that regions with similar functionality, that is, regions that are similarly modulated by various task paradigm - tend to be correlated in the BOLD spontaneous activity. On the other hand, regions with opposing functionality have been found to be negatively correlated in their spontaneous activity. Importantly, it was noted that resting state networks reflect the structure of the connections between brain regions. The information on the anatomical wiring of the brain are encoded in the Structural Connectivity are a_{ij} (SC) or anatomical connectivity that is a matrix whose elements are the weight of the connection between the region i and the region j . The SC is generally measured by the Diffusion Tensor Imaging (DTI) (basically, it relies on the alignment of the magnetic fields of water molecules in the axons fibers) and the DTI-derived structural connectivity can be compared to functional connectivity obtained by fMRI imaging. The comparison showed that although structural connectivity is a good predictor of functional connectivity (if there is a direct anatomical connection there is a functional connection) the opposite is not necessarily true. The interaction between these types of connectivity, and in particular if and how the structure gives rise to function in neuroscience are among the current neuroscience challenges [22]. This work puts the stress on the importance to go over the anatomical connectivity in order to predict the realistic functional connectivity. In fact, in chapter 6 we will show our simulation results, where a comparison between SC and FC id illustrated and we will see other influences on the resting state network dynamics, such as noise and criticality.

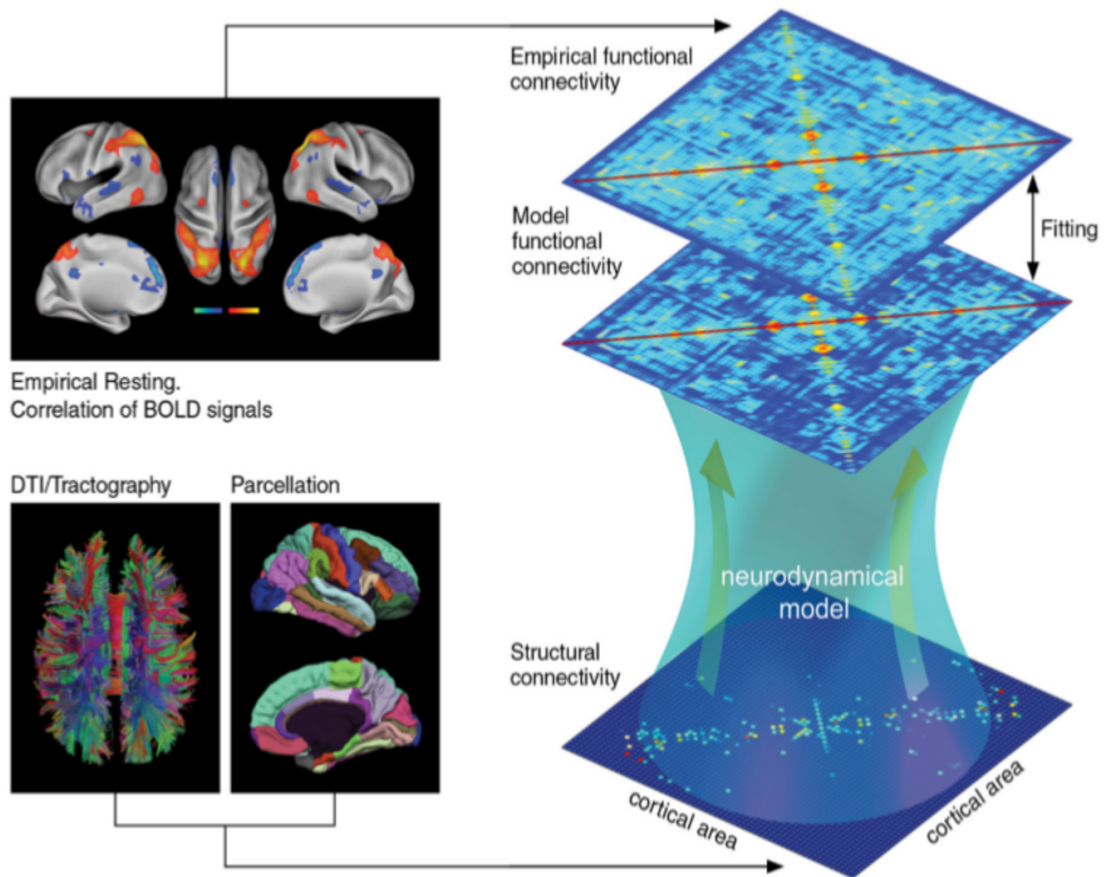


FIGURE 2.1: Linking anatomical connections and FC. Neuroanatomical connectivity data were obtained by DSI and tractography after averaging across subjects. Parcellation provides a connectivity matrix C linking the N cortical areas with clear anatomical landmarks. A neurodynamical model was then constructed using a set of stochastic differential equations coupled according to the connectivity matrix C . To validate the model, we compared the model spatiotemporal patterns to the ones observed in empirical data. In our case, the empirical FC was measured using fMRI BOLD activity. This framework enables us to study the link between anatomical structure and resting-state dynamics [14].

Chapter 3

Dynamical systems in Neuroscience

It is clear that the brain is a very complex system, hence its description requires the basic knowledge of dynamical systems. This fundamental theory permits us to understand the spatio-temporal evolution of the complicated neural networks.

In this chapter it is summarized the main dynamical system tools needed for the study of the resting state network dynamics of the next chapters. Indeed, we will give the mathematical framework to better understand our analysis and results. Firstly, we discuss the formalism that is at the heart of all dynamical sciences, namely the evolution equation. Such an expression ties the temporal unfolding of a system to its physical properties and is typically a differential equation. Secondly, we aim to motivate, illustrate and provide definitions for the language of dynamical systems theory integrating analysis and geometry, hence permitting the qualitative understanding and quantitative analysis of evolution equations. To this purpose we provide a short explanation of the basic terms of phase space analysis (equilibria and attractors) and a description of the basic bifurcation theory.

3.1 Basic notions of Dynamical Systems

The fluid nature of perceptual experience and the transient repetition of patterns in neurophysiological data attest to the dynamical character of neural activity. An approach to neuroscience that starts from this premise holds the potential to unite neuronal connectivity and brain activity by treating space and time in the same framework, that is analysing the evolution equations of some dynamical system. Dynamical systems theory is an area of mathematics used to describe the behaviour of the complex dynamical systems and its basic notion includes the following ingredients: a phase space S whose elements represent all the possible states of the system; time t , which may be discrete or continuous and an evolution law (that is, a rule that allows determination of the state at time t from the knowledge of the states at all previous times). Based on time, dynamical systems may be divided into two broad categories according to whether the time variable may be considered as continuous or discrete; hence, the dynamics of a given system is described by differential equations or finite-difference equations of the form

$$\frac{dx}{dt} = \dot{x} = X(x) \quad (3.1)$$

$$x_{t+1} = f(x_t) \quad (3.2)$$

To solve (3.1) and (3.2) we need to specify the initial state $x(0)$. In most examples, knowing the state at time t_0 allows determination of the state at any time $t > t_0$: in

this case the rule may be deterministic; conversely, when the evolution of the state is subject to random shocks the rule may be stochastic. Moreover, it is important to say that any system of differential equations of order higher than one can be written as a first-order system of higher dimensionality [21]. As we will handle mostly with non-linear differential equations and it knows that they can be notoriously intractable with regards to exact analytic solutions, a thorough understanding of their dynamics is very often possible by combining analysis and geometry. For any study of geometry, we require a space in which to embed our objects of study: the phase space, a differentiable manifold whose axes are spanned by the dynamical variables x of an evolution equation. The topology of the phase space is chosen to match the properties of these variables. We can think of a point in phase space as the instantaneous state $x(t)$ of our system. If we substitute this state into our evolution equation, we would get the instantaneous rate of change of the system $dx(t)/dt$ when in that state. This defines a tangent vector in the phase space, which will tell us how the system will evolve into its next state $x(t')$. More technically, a vector field assigns a vector to every point in phase space which is precisely the solution of the evolution equation at that point. Vector fields or phase portraits are often represented as arrows overlaid on the phase space (In mathematical language they are defined on a related space called the tangent bundle). An orbit or trajectory is a connected path through phase space which is always tangent to the vector field. Hence an orbit traces the time-dependent solution to a dynamical system through a succession of instantaneous states. It captures the manner in which a system will change according to the evolution equation. The starting point of such an orbit is called its initial condition [19]. Due to the uniqueness of the solutions, the trajectories cannot cross, so they partition or foliate the phase space.

3.2 Equilibria classification and attractors

In the next two paragraphs the central concepts of stability, either in one and two dimensions, are summarized from the textbook [20]. Let us start analysing the one-dimensional case. Continuous one-dimensional dynamical systems are usually written in the form

$$\dot{V} = F(V), \quad V(0) = V_0 \in \mathbb{R} \quad (3.3)$$

where V is a scalar time-dependent variable denoting the current state of the system, $\dot{V} = V_t = dV/dt$ is its derivative with respect to time t , F is a scalar function (its output is one-dimensional) that determines the evolution of the system and $V_0 \in \mathbb{R}$ is an initial condition in the real line. As we already said, finding explicit solutions is often impossible even for such simple systems as (3.3), but in many cases we just need qualitative understanding of the behaviour of (3.3) and how it depends on parameters and the initial state V_0 . The first step in the qualitative geometrical analysis of any one-dimensional dynamical system is to plot the graph of the function F . The next step is to find its equilibria or rest points, that is, the values of the state variable that:

$$F(V) = 0 \quad (3.4)$$

At each such point $\dot{V} = 0$, the state variable V does not change. If the initial value is near the equilibrium, the state variable may approach the equilibrium or diverge from it. We say that an equilibrium is asymptotically stable if all solutions starting sufficiently near the equilibrium will approach it as $t \rightarrow \infty$. Stability of an equilibrium is determined by the signs of the function F around it. The equilibrium is stable

when $F(V)$ changes the sign from “plus” to “minus” as V increases. Obviously, all solutions starting near such an equilibrium converge to it. Such an equilibrium “attracts” all nearby solutions, so it is called an attractor. A stable equilibrium point is the only type of attractor that can exist in one-dimension. A sufficient condition for an equilibrium to be stable is that the derivative of the function F with respect to V at the equilibrium is negative, provided the function is differentiable. We denote this derivative here by

$$\lambda = F'(V) \quad (3.5)$$

where V is an equilibrium. Conversely, positive slope λ implies instability. The parameter λ defined above is the simplest example of an eigenvalue of an equilibrium. If a one-dimensional system has two stable equilibrium points, then they must be separated by at least one unstable equilibrium point (this may not be true in multi-dimensional systems). An unstable equilibrium is sometimes called a repeller. Even though unstable equilibria are hard to see experimentally, they still play an important role in dynamics, since they separate attraction domains. In general, the basin (or domain) of attraction of an attractor is the set of all initial conditions that lead to the attractor. Moreover, unstable equilibria play the role of thresholds in one-dimensional bistable systems, such as in systems having two attractors, which is believed to describe the essence of the mechanism of bistability in many neurons. Suppose the state variable is initially at the stable equilibrium and suppose that perturbations can kick it around the equilibrium. Small perturbations may not kick it over the unstable equilibrium so that the state variable continues to be in the attraction domain: we refer to such perturbations as subthreshold. In contrast, we refer to perturbations as superthreshold if they are large enough to push the state variable over the unstable equilibrium so that it becomes attracted to the other stable state. The transition between two stable states separated by a threshold is relevant to the mechanism of excitability and generation of action potentials in many neurons. Systems having two (many) coexisting attractors are called bistable (multistable). Phase portraits depicts all stable and unstable equilibria, representative trajectories, and corresponding attraction domains in the system’s state and can be used to determine qualitative similarity of dynamical systems. In particular, two one-dimensional systems are said to be topologically equivalent when the phase portrait of one of them, treated as a piece of rubber, can be stretched or shrunk to fit the other one. Two systems having different numbers of equilibria cannot be topologically equivalent and, hence, they have qualitatively different dynamics. In computational neuroscience, it is usually faced quite complicated systems describing neuronal dynamics. An useful strategy is to replace such systems with simpler ones having topologically equivalent phase portraits. Quite often we cannot find a simpler system that is topologically equivalent to our neuronal model on the entire state line. In this case, we make a sacrifice: we restrict our analysis to a small neighborhood of the line \mathbb{R} , and study behaviour locally in this neighbourhood. An important tool in the local analysis of dynamical systems is the Hartman-Grobman theorem, which says that a nonlinear one-dimensional system $\dot{V} = F(V)$ sufficiently near an equilibrium $V = V_{eq}$ is locally topologically equivalent to the linear system

$$\dot{V} = \lambda(V - V_{eq}) \quad (3.6)$$

provided the eigenvalue

$$\lambda = F'(V_{eq}) \quad (3.7)$$

at the equilibrium is nonzero, that is, the slope of $F(V)$ is nonzero. Such an equilibrium is called hyperbolic. Thus, nonlinear systems near hyperbolic equilibria behave as if they were linear. The solution of the linearized system (3.3) with an initial condition $V(0) = V_0$ is $V(t) = V_{eq} + e^{\lambda t}(V_0 - V_{eq})$. If the eigenvalue $\lambda < 0$, then $e^{\lambda t} \rightarrow 0$ and $V(t) \rightarrow V_{eq}$ as $t \rightarrow \infty$, so that the equilibrium is stable. Conversely, if $\lambda > 0$, then $e^{\lambda t} \rightarrow \infty$ meaning that the initial displacement, $V_0 - V_{eq}$, grows with time and the equilibrium is unstable. Thus, the linearization predicts qualitative dynamics at the equilibrium, and the quantitative rate of convergence/divergence to/from the equilibrium. If the eigenvalue $\lambda = 0$, then the equilibrium is non-hyperbolic, and analysis of the linearized system $\dot{V} = 0$ cannot describe the behavior of the nonlinear system. Typically, non-hyperbolic equilibria arise when the system undergoes a bifurcation (see next section) and to study stability, we need to consider higher-order terms of the Taylor series of $F(V)$ at V_{eq} .

In two dimensional system there are more properties and they are characterized with a richer behaviour. Two-dimensional dynamical systems, also called planar systems, are often written in the form

$$\begin{aligned}\dot{x} &= f(x, y), \\ \dot{y} &= g(x, y)\end{aligned}\tag{3.8}$$

where the functions f and g describe the evolution of the two-dimensional state variable $(x(t), y(t))$. For any point (x_0, y_0) on the phase plane, the vector $(f(x_0, y_0), g(x_0, y_0))$ indicates the direction of change of the state variable. Since each point on the phase plane (x, y) has its own vector (f, g) , the system above is said to define a vector field on the plane and it provide geometrical information about the joint evolution of state variables. The set of points where the vector field changes its horizontal direction is called the x -nullcline, and it is defined by the equation $f(x, y) = 0$. Indeed, at any such point x neither increases nor decreases because $\dot{x} = 0$. The x -nullcline partitions the phase plane into two regions where x moves in opposite directions. Similarly, the y -nullcline is defined by the equation $g(x, y) = 0$, and it denotes the set of points where the vector field changes its vertical direction. This nullcline divides the phase plane into two regions where y either increases or decreases. Therefore, the x - and y -nullclines partition the phase plane into four different regions so that they represent the 'skeleton' of the phase portrait. Each point of intersection of the nullclines is an equilibrium point, since $f(x, y) = g(x, y) = 0$, and hence $\dot{x} = \dot{y} = 0$. A trajectory that

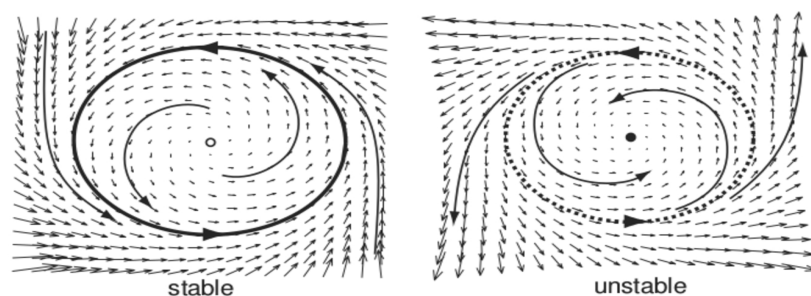


FIGURE 3.1: An illustration of limit cycles.

forms a closed loop is called a periodic trajectory or a periodic orbit. An isolated periodic trajectory is called a limit cycle. The existence of limit cycles is a major feature of two-dimensional systems that cannot exist in one dimension. If the initial point is on a limit cycle, then the solution $(x(t), y(t))$ stays on the cycle forever, and the

system exhibits periodic behaviour. A limit cycle is said to be asymptotically stable if any trajectory with the initial point sufficiently near the cycle approaches the cycle as $t \rightarrow \infty$. Such asymptotically stable limit cycles are often called limit cycle attractors, since they “attract” all nearby trajectories. The stable limit cycle in Fig.3.1 is an attractor. While the unstable limit cycle in is often called a repeller, since it repels all nearby trajectories. Notice that there is always at least one equilibrium inside any limit cycle on a plane. An important step in the analysis of any dynamical system is to find its equilibria, that is, points where

$$\begin{aligned} f(x, y) &= 0 \\ g(x, y) &= 0 \end{aligned} \quad (3.9)$$

and point (x, y) is said an equilibrium. As mentioned before, equilibria are intersections of nullclines. If the initial point is near the equilibrium, then the trajectory may converge to or diverge from the equilibrium, depending on its stability. For instability it suffices to have at least one trajectory that diverges from the equilibrium no matter how close the initial condition is to the equilibrium. To determine the stability of an equilibrium, we need to look at the behaviour of the two-dimensional vector field in a small neighbourhood of the equilibrium. Quite often visual inspection of the vector field does not give conclusive information about stability. However, many questions regarding the stability of the equilibrium can be answered by considering the corresponding linear system

$$\begin{aligned} \dot{u} &= au + bw \\ \dot{w} &= cu + dw \end{aligned} \quad (3.10)$$

where $u = x - x_0$ and $w = y - y_0$ are the deviations from the equilibrium, and the higher-order terms are neglected. We can write this system in the vector form

$$\dot{G} = LG \quad (3.11)$$

where $\dot{G} = (\dot{u}, \dot{w})^T$, $G = (u, w)^T$ and L is the Jacobian matrix. In general, 2×2 matrices have two eigenvalues with distinct (independent) eigenvectors: v_1 and v_2 . In this case a general solution of the linear system has the form

$$(u(t), w(t))^T = c_1 e^{\lambda_1 t} v_1 + c_2 e^{\lambda_2 t} v_2 \quad (3.12)$$

where c_1 and c_2 are constants that depend on the initial condition. This formula is valid for real and complex-conjugate eigenvalues. When both eigenvalues are negative (or have negative real parts), $u(t) \rightarrow 0$ and $w(t) \rightarrow 0$, meaning $x(t) \rightarrow x_0$ and $y(t) \rightarrow y_0$, so that the equilibrium (x_0, y_0) is exponentially (and hence asymptotically) stable. It is unstable when at least one eigenvalue is positive or has a positive real part. An equilibrium whose Jacobian matrix does not have zero eigenvalues or eigenvalues with zero real parts is called hyperbolic. Such an equilibrium can be stable or unstable. Also in two dimension the Hartman-Grobman theorem is valid. There are three major types of equilibria (see Fig 3.2):

- Node. The eigenvalues are real and of the same sign. The node is stable when the eigenvalues are negative, and unstable when they are positive. The trajectories tend to converge to or diverge from the node along the eigenvector corresponding to the eigenvalue having the smallest absolute value.
- Saddle. The eigenvalues are real and of opposite signs. Saddles are always

unstable, since one of the eigenvalues is always positive. Most trajectories approach the saddle equilibrium along the eigenvector corresponding to the negative (stable) eigenvalue and then diverge from it along the eigenvector corresponding to the positive (unstable) eigenvalue.

- **Focus.** The eigenvalues are complex-conjugate. Foci are stable when the eigenvalues have negative real parts, and unstable when the eigenvalues have positive real parts. The imaginary part of the eigenvalues determines the frequency of rotation of trajectories around the focus equilibrium.

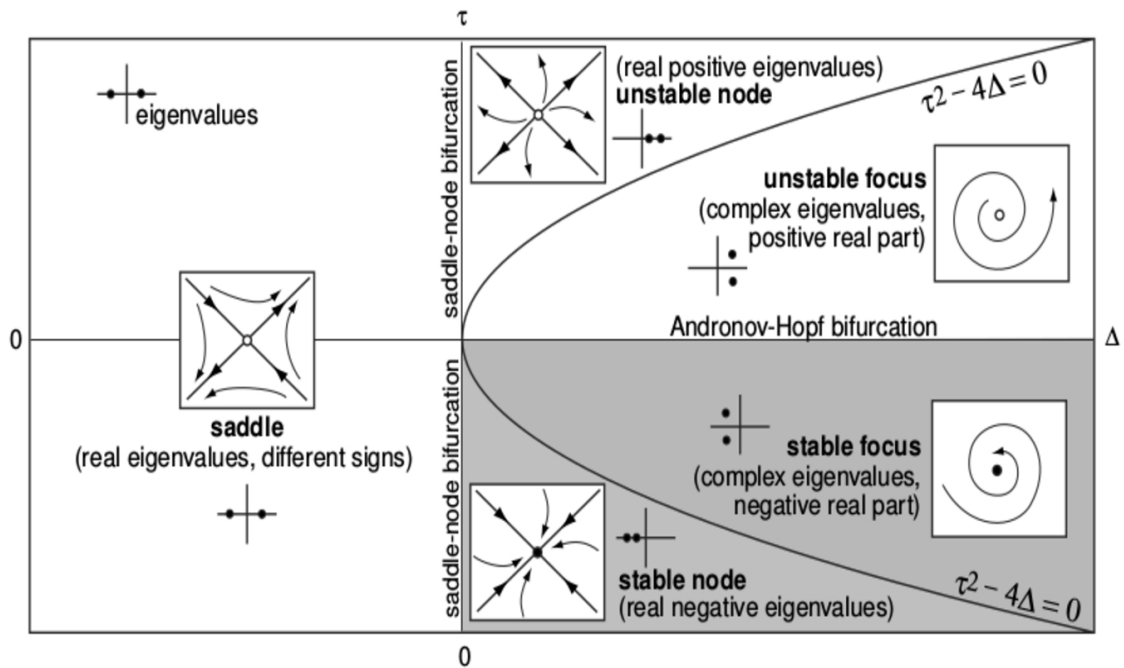


FIGURE 3.2: Classification of the equilibria in two dimensional systems.

Nonlinear two-dimensional systems can have many coexisting attractors (multistable systems). In contrast with one-dimensional systems, in two-dimensional systems unstable equilibria do not necessarily separate attraction domains. Nevertheless, they play an important role in defining the boundary of attraction domains. In both cases the attraction domains are separated by a pair of trajectories, called separatrices, which converge to the saddle equilibrium. Such trajectories form the stable manifold of a saddle point. Locally, the manifold is parallel to the eigenvector corresponding to the negative (stable) eigenvalue. Similarly, the unstable manifold of a saddle is formed by the two trajectories that originate exactly from the saddle (or approach the saddle if the time is reversed). Locally, the unstable manifold is parallel to the eigenvector corresponding to the positive (unstable) eigenvalue. We say that a trajectory is heteroclinic if it originates at one equilibrium and terminates at another equilibrium. A trajectory is homoclinic if it originates and terminates at the same equilibrium. These types of trajectories play an important role in geometrical analysis of dynamical systems. Heteroclinic trajectories connect unstable and stable equilibria, and they are ubiquitous in dynamical systems having two or more equilibrium points. In contrast, homoclinic trajectories are rare. Although uncommon, homoclinic trajectories indicate that the system undergoes a bifurcation.

3.3 Bifurcations

The final and most advanced step in the qualitative analysis of any dynamical system is the bifurcation analysis. In general, a system is said to undergo a bifurcation when its phase portrait changes qualitatively. Qualitative change of the phase portrait may or may not necessarily reveal itself in a qualitative change of behaviour, depending on the initial conditions. When mathematicians talk about bifurcations, they assume that all initial conditions could be sampled, in which case bifurcations do result in a qualitative change of behaviour of the system as a whole. In general, a dynamical system may depend on a vector of parameters, say p . A point in the parameter space, say $p = a$, is said to be a regular or non-bifurcation point, if the system's phase portrait at $p = a$ is topologically equivalent to the phase portrait at $p = c$ for any c sufficiently close to a . Any point in the parameter space that is not regular is called a bifurcation point. Namely, a point $p = b$ is a bifurcation point if the system's phase portrait at $p = b$ is not topologically equivalent to the phase portrait at a point $p = c$, no matter how close c is to b . The saddle-node (also known as fold or tangent) bifurcation is one of the simplest bifurcations. In general, a one-dimensional system $\dot{V} = F(V, I)$, having an equilibrium point $V = V_{sn}$ for some value of the parameter $I = I_{sn}$ (i.e., $F(V_{sn}, I_{sn}) = 0$), is said to be at a saddle-node bifurcation if the following mathematical conditions, illustrated in Fig.3.3, are satisfied:

- **Non-hyperbolicity.** The eigenvalue λ at V_{sn} is zero; that is, $\lambda = F_V(V, I_{sn}) = 0$ (at $V = V_{sn}$), where $F_V = \partial F / \partial V$. Equilibria with zero or pure imaginary eigenvalues are called non-hyperbolic. Geometrically, this condition implies that the graph of F has horizontal slope at the equilibrium.
- **Non-degeneracy.** The second-order derivative with respect to V at V_{sn} is nonzero; that is, (at $V = V_{sn}$), $F_{VV}(V, I_{sn}) \neq 0$. Geometrically, this means that the graph of F looks like the square parabola V^2 .
- **Transversality.** The function $F(V, I)$ is non-degenerate with respect to the bifurcation parameter I ; that is, $F_I(V_{sn}, I) \neq 0$ (at $I = I_{sn}$), where $F_I = \partial F / \partial I$. Geometrically, this means that as I changes past I_{sn} , the graph of F approaches, touches, and then intersects the V -axis.

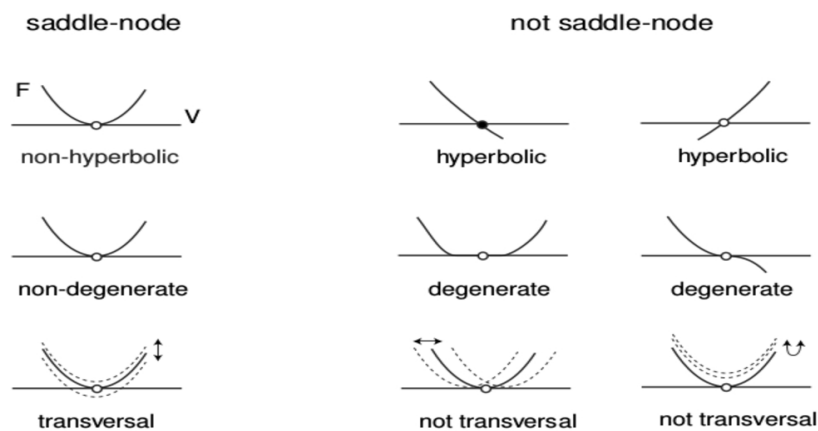


FIGURE 3.3: Condition for a saddle-node bifurcation.

The number of conditions involving strict equality is called the codimension of a bifurcation and the saddle-node bifurcation has codimension 1. Codimension-1 bifurcations can be reliably observed in systems with one parameter. It is an easy exercise to check that the one-dimensional system $\dot{V} = I + V^2$ is at saddle-node bifurcation when $V = 0$ and $I = 0$. This system is called the topological normal form for saddle-node bifurcation. All the systems near saddle-node bifurcations possess certain universal features that do not depend on particulars of the systems. Consequently, all neural systems near such a bifurcation share common neurocomputational properties. Here we take a look at one such property – slow transition through the ruins (or ghost) of the resting state attractor. In the example in Fig.3.4 the system has only one attractor, the excited state, and any solution starting from an arbitrary initial condition should quickly approach this attractor. However, the solutions starting from the initial conditions around the shaded area do not seem to hurry. Instead, they slow down and spend a considerable amount of time in the voltage range corresponding to the resting state, as if the state were still present. The closer I is to the bifurcation value, the more time the membrane potential spends in the neighbourhood of the resting state.

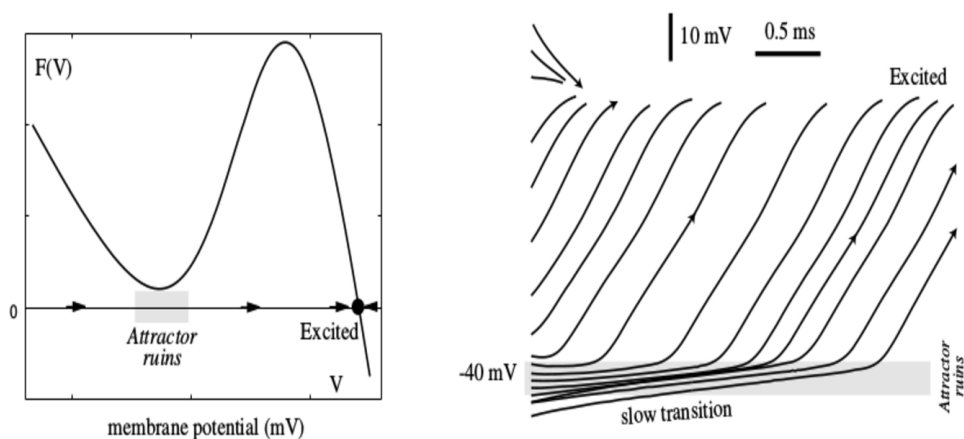


FIGURE 3.4: Ghost attractor.

The final step in the geometrical bifurcation analysis of one-dimensional systems is the analysis of bifurcation diagrams, which we do in Fig. 3.5(right). To draw the bifurcation diagram, we determine the locations of the stable and unstable equilibria for each value of the parameter I and plot them as white or black circles in the (I, V) plane in Fig. 3.5(right). The equilibria form two branches that join at the fold point corresponding to the saddle-node bifurcation (hence the alternative name fold bifurcation). As the bifurcation parameter I varies from left to right, passing through the bifurcation point, the stable and unstable equilibria coalesce and annihilate each other. As the parameter varies from right to left, two equilibria – one stable and one unstable – appear from a single point. Thus, depending on the direction of movement of the bifurcation parameter, the saddle-node bifurcation explains disappearance or appearance of a new stable state. In any case, the qualitative behaviour of the systems changes exactly at the bifurcation point.

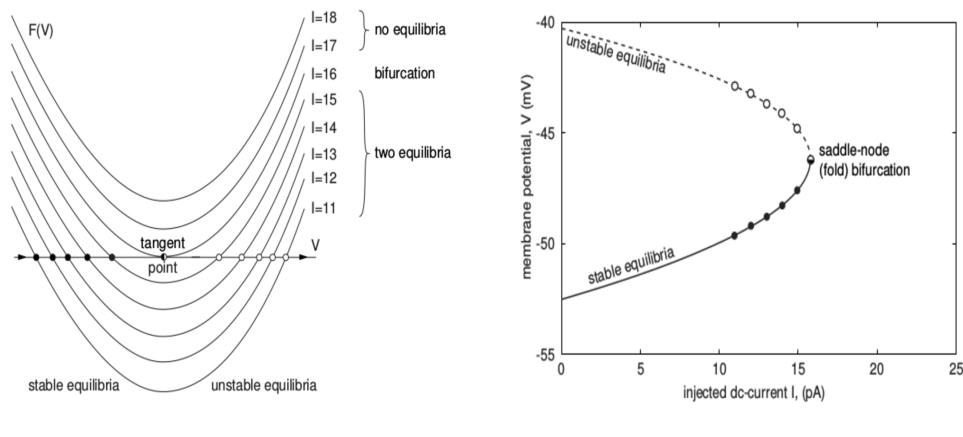


FIGURE 3.5: Bifurcation diagram.

In two dimension the saddle-node bifurcation, is more or less the same than for one dimensional systems. In two dimension there is another kind of bifurcation, that is the transition from stable to unstable focus, called the Andronov-Hopf bifurcation (see Fig. 3.2). It occurs when the eigenvalues become purely imaginary and they can be supercritical or subcritical. The former correspond to birth of a small-amplitude limit cycle attractor, the latter correspond to the death of an unstable limit cycle. In summary, Hopf bifurcations are of very high importance for an understanding of the neural activity as they explain the onset and nature of oscillatory behaviour. Supercritical Hopf bifurcations lead to the appearance of small amplitude periodic oscillations. Subcritical Hopf bifurcations result immediately in a large amplitude limit cycle. Supercritical and subcritical Andronov-Hopf bifurcations in neurons result in slightly different neurocomputational properties. In contrast, the saddle-node and Andronov-Hopf bifurcations result in dramatically different neurocomputational properties:

- Neurons near a saddle-node bifurcation act as integrators – they prefer high-frequency input. The higher the frequency of the input, the sooner they fire.
- Neural systems near Andronov-Hopf bifurcations have damped oscillatory potentials and act as resonators – they prefer oscillatory input with the same frequency as that of damped oscillations. Increasing the frequency may delay or even terminate their response.

Whereas local bifurcations deal with the loss of asymptotic stability of fixed points - and are hence concerned with the dynamics in local neighborhoods of attractors - global bifurcations can only be understood by studying the properties of the vector field outside of such neighborhoods. They occur when an attractor loses structural stability. Their nature depends upon the “skeleton” of the phase space – the nullclines, homoclines and heteroclines.

Chapter 4

From neurobiology to dynamical models

Biological systems are among the most complex systems in nature and the number of components of such systems is enormous. For instance, each neuron can have up to 10^5 inward connections and, taking into account that about 100 billion neurons are present in the human brain, they are organized into a huge and complex network of connections, which could theoretically reach 10^{16} . The activity of this 'connectome' is the responsible of all the mental ability, as perception, consciousness, memory and so on. Therefore, in order to understand the brain dynamics, we need to deep analyse the biological background that permit all of these phenomena. Only after we can build realistic theoretical representations of such system.

In this chapter we briefly show the neurobiology and neurophysiology of the brain at each spacial scale:

- The micro-scale, where we take into account the way of exchanging and integrating information between the computing elements of the brain: the neurons.
- The meso-scale, where we describe the dynamics of neural population, a group of similar neurons which share the same behaviour so that can be studied as a sole system.
- The macro-scale, where we give information about the whole brain dynamics and about the interactions between large-scale neural systems, such as cortical regions.

4.1 The Neurons

The aim of this section is to introduce several elementary notions of neuron anatomy and physiology to provide the reader with a minimum of information necessary to appreciate the biological reason of the theoretical work presented in this thesis. Due to the limitations of space we cannot give a comprehensive introduction into such a complex field as neurobiology. The presentation of the biological background in this chapter is therefore highly selective and simplistic. For an in-depth discussion of we refer the reader to the standard handbook of neurobiology [9].

Over the past hundred years, biological research has accumulated an enormous amount of detailed knowledge about the structure and function of the brain. The elementary processing units in the central nervous system are neurons which are connected to each other in an intricate pattern. A tiny portion of such a network of neurons is sketched in Fig. 4.1 which shows a drawing by Ramón y Cajal, one of the pioneers of neuroscience, made at the begin of 20th century. This picture can

only give a glimpse of the network of neurons in the cortex. In all areas, however, neurons of different sizes and shapes form the basic elements. Besides, the various types of neuron there is a large number of ‘supporter’ cells, so-called glia cells, that are required for energy supply and structural stabilization of brain tissue. Since glia cells are not directly involved in information processing, we will not discuss them any further. We will also neglect a few rare subtypes of neuron. Throughout this work we concentrate on spiking neurons only.

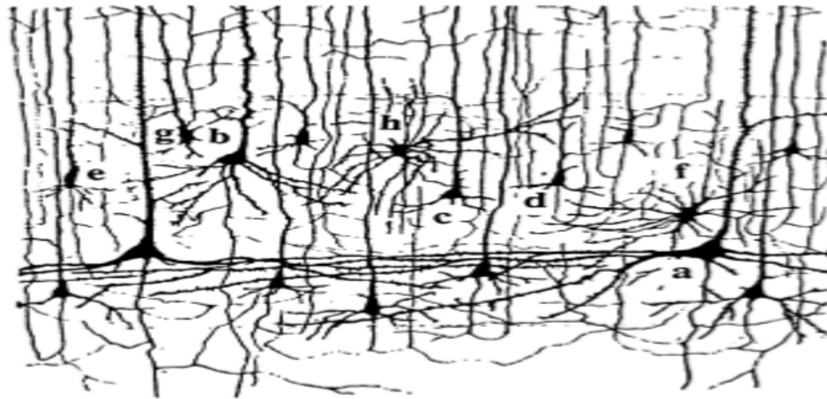


FIGURE 4.1: This reproduction of a drawing of Ramón y Cajal shows a few neurons in the mammalian cortex that he observed under the microscope.

A typical neuron can be divided into three functionally distinct parts, called dendrites, soma, and axon (see Fig. 4.2):

- The dendrites play the role of the ‘input device’ that collects signals from other neurons and transmits them to the soma.
- The soma is the ‘central processing unit’ that performs an important non-linear processing step: if the total input exceeds a certain threshold, then an output signal is generated.
- The output signal is taken over by the ‘output device’, the axon, which delivers the signal to other neurons.

Neurons are, just as other cells, enclosed by a membrane which separates the interior of the cell from the extracellular space. Inside the cell the concentration of ions is different from that in the surrounding liquid. The difference in concentration generates an electrical potential which plays an important role in neuronal dynamics. In this section, we want to provide some background information and give an intuitive explanation of the equilibrium potential. From the theory of thermodynamics, it is known that the probability that a molecule takes a state of energy E is proportional to the Boltzmann factor $p(E) \propto \exp(-E/kT)$ where k is the Boltzmann constant and T the temperature. Let us consider positive ions with charge q in a static electrical field. Their energy at location x is $E(x) = q u(x)$ where $u(x)$ is the potential at x . The probability to find an ion in the region around x is therefore proportional to $\exp[-q u(x)/kT]$. Since the number of ions is huge, we may interpret the probability as a ion density. For ions with positive charge $q > 0$, the ion density is therefore higher in regions with low potential u . A difference in ion density generates a difference

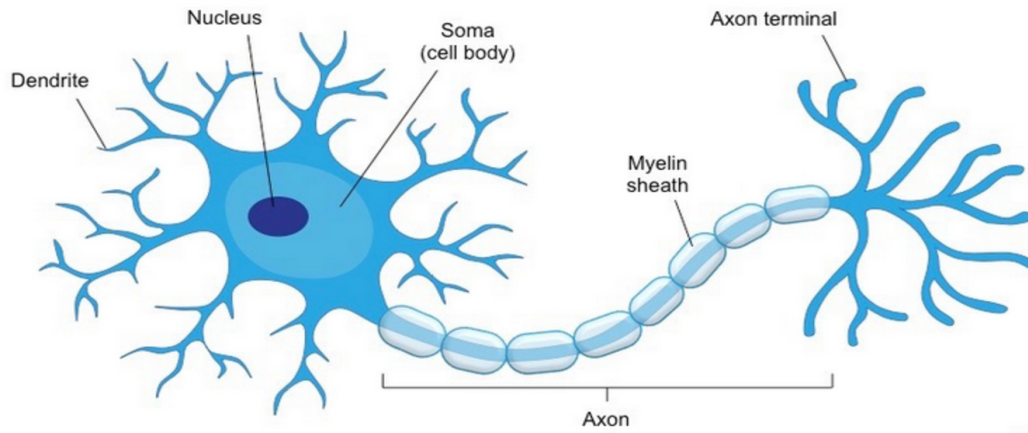


FIGURE 4.2: Sketch of the structure of a typical neuron.

Δu in the electrical potential. We consider two regions of ions with concentration n_1 and n_2 , respectively. It is straightforward that, at equilibrium, the concentration difference generates a voltage

$$\Delta u = \frac{kT}{q} \ln \frac{n_2}{n_1} \quad (4.1)$$

which is called the Nernst potential. Now we try to explain the concept of reversal potential with an useful example. Ion concentrations in the intra-cellular liquid differ from that of the surround. For example, the sodium concentration inside the cell (≈ 60 mM/l) is lower than that in the extracellular liquid (≈ 440 mM/l). On the other hand, the potassium concentration inside is higher (≈ 400 mM/l) than in the surround (≈ 20 mM/l). Let us concentrate for the moment on sodium ions. At equilibrium the difference in concentration causes a Nernst potential E_{Na} of about +50 mV. That is, at equilibrium the interior of the cell has a positive potential with respect to the surround. The interior of the cell and the surrounding liquid are in contact through ion channels where Na^+ ions can pass from one side of the membrane to the other. If the voltage difference Δu is smaller than the value of the Nernst potential E_{Na} , more Na^+ ions flow into the cell so as to decrease the concentration difference. If the voltage is larger than the Nernst potential ions would flow out of the cell. Thus the direction of the current is reversed when the voltage Δu passes E_{Na} . For this reason, E_{Na} is called the reversal potential. So far we have considered just sodium, but in real cells, this and other ion types, as potassium, are simultaneously present and contribute to the voltage across the membrane. It is found experimentally that the resting potential of the membrane is about $u_{rest} \approx -65$ mV. Since $E_K < u_{rest} < E_{Na}$, potassium ions will, at the resting potential, flow out of the cell while sodium ions flow into the cell. The active ion pumps balance this flow and transport just as many ions back as pass through the channels. The value of u_{rest} is determined by the dynamic equilibrium between the ion flow through the channels (permeability of the membrane) and active ion transport (efficiency of the ion pumps) [25].

The nerve cell peculiarity is the electrical excitability. In electrically excitable cell a sufficiently large depolarization of the membrane potential can evoke an action potential, during which the membrane potential changes quickly (for an example look at Fig. 4.5 b). The neuronal signals consist of short electrical pulses and can be observed by placing a fine electrode close to the soma or axon of a neuron. The

pulses, so-called action potentials or spikes, have an amplitude of about 100 mV and typically a duration of 1-2 ms. The form of the pulse does not change as the action potential propagates along the axon. A chain of action potentials emitted by a single neuron is called a spike train – a sequence of stereotyped events which occur at regular or irregular intervals. Since all spikes of a given neuron look alike, the form of the action potential does not carry any information. Rather, it is the number and the timing of spikes which matter. Action potentials in a spike train are usually well separated. Even with very strong input, it is impossible to excite a second spike during or immediately after a first one. The minimal distance between two spikes defines the absolute refractory period of the neuron. The absolute refractory period is followed by a phase of relative refractoriness where it is difficult, but not impossible to excite an action potential.

The rapid changes in membrane potential are mediated by ion channels, a class of integral membrane proteins found in all cells of the body. The ion channels of nerve cells are optimally tuned for rapid information processing. The channels of nerve cells are also heterogeneous, so that different types of channels in different parts of the nervous system can carry out specific signalling tasks. Activated transmembrane ion channels allow ions flow into or out of cells. In neurons, these channels promote neurotransmission by altering polarization of the neuronal membrane. Neuronal ion channel activation occurs in either a voltage-gated or a ligand-gated manner. Voltage-gated channels are activated by changes in the electrical potential across a membrane. Ligand-gated channels are activated by the binding a specific ligand. Each channel is usually selective for one ion type, such as sodium, calcium, potassium, or chloride.

The site where the axon of a presynaptic neuron makes contact with the dendrite (or soma) of a postsynaptic cell is the synapse. The most common type of synapse in the vertebrate brain is a chemical synapse. At a chemical synapse, the axon terminal comes very close to the postsynaptic neuron, leaving only a tiny gap between pre- and postsynaptic cell membrane, called the synaptic cleft. When an action potential arrives at a synapse, it triggers a complex chain of biochemical processing steps that lead to a release of neurotransmitter from the presynaptic terminal into the synaptic cleft. As soon as transmitter molecules have reached the postsynaptic side, they will be detected by specialized receptors in the postsynaptic cell membrane and open (either directly or via a biochemical signaling chain) specific channels so that ions from the extracellular fluid flow into the cell. The ion influx, in turn, leads to a change of the membrane potential at the postsynaptic site so that, in the end, the chemical signal is translated into an electrical response. The voltage response of the postsynaptic neuron to a presynaptic action potential is called the postsynaptic potential. Apart from chemical synapses neurons can also be coupled by electrical synapses, so-called gap junctions. Specialized membrane proteins make a direct electrical connection between the two neurons. Synapses can be classified as excitatory or inhibitory. If the membrane potential of the postsynaptic cell increases, the postsynaptic neuron is driven towards its excited state, and the synapse is considered excitatory. On the other hand, inhibitory synapse is associated with a decrease in membrane potential, which drives the postsynaptic neuron towards its resting state membrane potential. The three principal receptors are AMPA, NMDA and GABA. The AMPA current activates and deactivates rapidly. In contrast, the NMDA current activates and deactivates slowly and it has a voltage dependence controlled by the extracellular magnesium concentration. The GABA is the principal inhibitory neurotransmitter.

4.2 Neuron dynamics

Neurons are traditionally seen as the building blocks of the brain. It hence makes sense to gain some insight into their dynamics – and functional interactions – at the microscopic scale at which they reside before moving into the larger scales, which we will do in next sections. The “foundation stone” of microscopic models are the conductance-based Hodgkin-Huxley model and its derivatives. Our objective here will be to quickly move from the full model to a two dimensional approximation and then explicate the onset of neuronal firing as a dynamical bifurcation. Throughout we will briefly explain others important neuronal models.

A biological neuron model, also known as a spiking neuron model, is a mathematical description of the properties of certain cells in the nervous system that generate sharp electrical potentials across their cell membrane and, ultimately, they aim to explain the mechanisms underlying the operation of the nervous system. The most extensive experimental inquiry in this category of models was made by Hodgkin–Huxley in the early 1950s [12] using an experimental set up that punctured the cell membrane and allowed to force a specific membrane voltage/current. In this work the leak integrate-and-fire model (LIF) is treated before the Hodgkin-Huxley model, although the LIF model is more recent and it is a simplification of the Hodgkin-Huxley model; it has been preferred following the sequence that make easier the understanding instead that following the chronological order.

Modelling a neuron as an electric circuit was firstly investigated by Lapicque over 100 years ago, and his model is known today as integrate-and-fire model or single compartment model. Lapicque’s idea captures two of the most important aspects of neuronal excitability: the integration of the incoming signals and the generation of the spike once a certain threshold is exceeded. This is obtained by considering the neuron an electric circuit consists of a capacitor, a threshold detector and a switch (without the resistor), and by describing the variation in time of the membrane potential with a single variable V :

$$C \frac{dV}{dt} = \frac{dQ}{dt} \quad (4.2)$$

When an input current is applied, the membrane voltage increases with time until it reaches a constant threshold V_{th} ; at this point a delta function spike occurs, the switch closes and shunts the capacitor that resets the voltage to its resting potential V_L . The main shortcoming of the integrate and fire model is that it has no time-dependent memory. If the circuit receives a below-threshold signal, the voltage boosts forever until it fires again. This characteristic clearly does not reflect the observed neuronal behaviour. In the leak fire-and-integrate model, the memory problem is solved by adding a “leak” term to the membrane potential, reflecting the diffusion of ions that occurs through the membrane when the cell does not reach the proper balance. In the previous electrical circuit, the LIF model is implemented adding a resistor in parallel with the capacitor; hence the equation 4.3 can be written as:

$$C \frac{dV}{dt} = -g[V(t) - V_L] + \frac{dQ}{dt} \quad (4.3)$$

where g is the conductance.

Hodgkin and Huxley [12] performed experiments on the giant axon of the squid and found three different types of ion current, viz., sodium, potassium, and a leak current that consists mainly of Cl^- ions. Specific voltage-dependent ion channels, one for sodium and another one for potassium, control the flow of those ions through the cell membrane. The leak current takes care of other channel types which are not

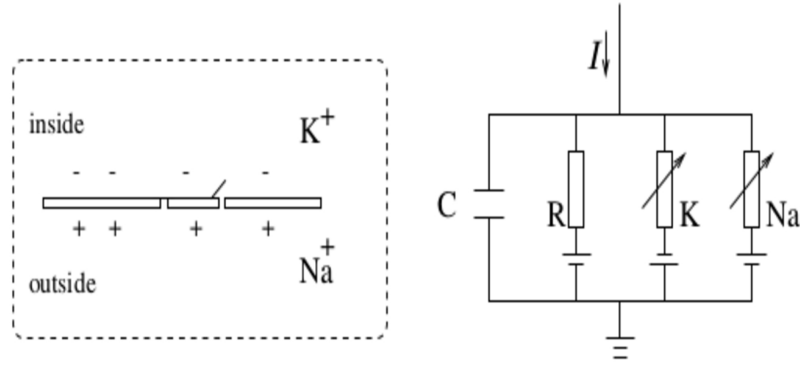


FIGURE 4.3: Schematic diagram for the Hodgkin-Huxley model.

described explicitly. The Hodgkin-Huxley model can be understood with the help of Fig. 4.3. The semipermeable cell membrane separates the interior of the cell from the extracellular liquid and acts as a capacitor. If an input current $I(t)$ is injected into the cell, it may add further charge on the capacitor, or leak through the channels in the cell membrane. Because of active ion transport through the cell membrane, the ion concentration inside the cell is different from that in the extracellular liquid. The Nernst potential generated by the difference in ion concentration is represented by a battery. Let us now translate the above considerations into mathematical equations. The conservation of electric charge on a piece of membrane implies that the applied current $I(t)$ may be split in a capacitive current I_C which charges the capacitor C and further components I_k which pass through the ion channels. Hence

$$C \frac{du}{dt} = - \sum_{k=1}^N I_k(t) + I(t) \quad (4.4)$$

As mentioned above, the Hodgkin-Huxley model describes three types of channel. All channels may be characterized by their resistance or, equivalently, by their conductance. The leakage channel is described by a voltage-independent conductance $g_L = 1/R$; the conductance of the other ion channels is voltage and time dependent. If all channels are open, they transmit currents with a maximum conductance g_{Na} or g_K , respectively. Normally, however, some of the channels are blocked. The probability that a channel is open is described by additional variables m , n , and h . The combined action of m and h controls the Na^+ channels. The K^+ gates are controlled by n . Specifically, Hodgkin and Huxley formulated the three current components as

$$\sum_{k=1}^N I_k = g_{Na} m^3 h (u - E_{Na}) + g_K n^4 (u - E_K) + g_L (u - E_L) \quad (4.5)$$

The parameters E_{Na} , E_K , and E_L are the reversal potentials. Reversal potentials and conductances are empirical parameters. In Table 4.1 we have summarized the original values reported by Hodgkin and Huxley [12]. The three variables m , n , and h are called gating variables. They evolve according to the differential equations

$$\begin{aligned} \dot{m} &= \alpha_m(u)(1 - m) - \beta_m(u)m \\ \dot{n} &= \alpha_n(u)(1 - n) - \beta_n(u)n \\ \dot{h} &= \alpha_h(u)(1 - h) - \beta_h(u)h \end{aligned} \quad (4.6)$$

x	$E_x(\text{mV})$	$g_x(\text{mS/cm}^2)$	x	$\alpha_x(u/\text{mV})$	$\beta_x(u/\text{mV})$
Na	115	120	n	$(0.1-0.01u)/[\exp(1-0.1u)-1]$	$0.125\exp(-u/80)$
K	-12	36	m	$(2.5-0.1u)/[\exp(2.5-0.1u)-1]$	$4\exp(-u/18)$
L	10.6	0.3	h	$0.07/[\exp(-u/20)]$	$1/[\exp(3-0.1u)+1]$

TABLE 4.1: The parameters of the Hodgkin-Huxley equations. The voltage scale is shifted so that the resting potential vanishes.

The various functions α and β , given in table 4.1, are empirical functions of u that have been adjusted by Hodgkin and Huxley to fit the data of the giant axon of the squid. Eqs. (4.5) – (4.7) with the values given in Table 4.1 define the Hodgkin-Huxley model. In order to get a better understanding of the three equations (4.7), it is convenient to rewrite each of the equations in the form

$$\dot{x} = -\frac{1}{\tau}x(u)[x - x_0(u)] \quad (4.7)$$

where x stands for m , n , or h . For fixed voltage u , the variable x approaches the value $x_0(u)$ with a time constant $\tau_x(u)$. The asymptotic value $x_0(u)$ and the time constant $\tau_x(u)$ are given by the transformation $x_0(u) = \alpha_x(u)/[\alpha_x(u)+\beta_x(u)]$ and $\tau_x(u)=[\alpha_x(u) + \beta_x(u)]^{-1}$. Using the parameters given by Hodgkin and Huxley we have plotted in Fig. 4.4 the functions $x_0(u)$ and $\tau_x(u)$ [25].

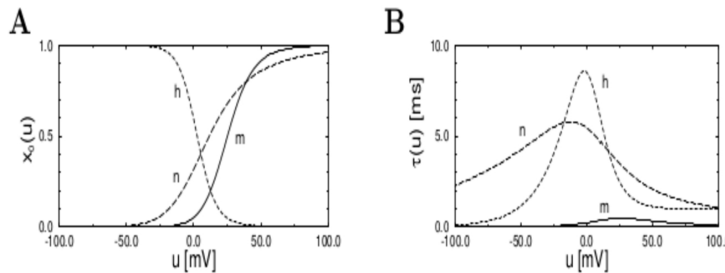


FIGURE 4.4: Equilibrium function (A) and time constant (B) for the three variables m , n , h . The resting potential is at $u = 0$.

The Hodgkin-Huxley model is a beautiful juncture of empirical and mathematical analysis that offers an explanation of neural firing and that captures quantitatively the complex shape of a neural depolarization. However, much of the qualitative behaviour can be captured by good approximations of the model. An essential ingredient of a neural firing is a fast depolarizing current such as Na^+ – which is turned on subsequent to a synaptic current – and a slow repolarizing current such as K^+ – which restores the resting membrane potential. These in turn are facilitated by the existence of slow and fast ion channels of the respective species, $\tau_m(V) \ll \tau_n(V)$. The depolarizing current represents positive feedback (i.e. is self promoting) and, if a threshold is reached before a sufficient number of slower K^+ channels are open, the cell depolarizes. By contrast, the Na^+ inactivation channel plays less of a “brute force” role and can be ignored. The requirement of a “fast” depolarizing current and

a slow repolarizing current can be met in a two dimensional (“planar”) system,

$$\frac{dV}{dt} = g_{Na}m_{\infty}(V)(V - V_{Na}) + g_Kn(V)(V - V_K) + g_L(V - V_L) + I \quad (4.8)$$

where the dynamics of the slow repolarizing K^+ is given by

$$\frac{dn}{dt} = \frac{(n_{\infty} - n)}{\tau_n} \quad (4.9)$$

and the steady state currents given by

$$\begin{aligned} n_{\infty}(V) &= \frac{n_{max}}{1 + \exp((v_n - v)/\sigma)} \\ m_{\infty}(V) &= \frac{m_{max}}{1 + \exp((v_m - v)/\sigma)} \end{aligned} \quad (4.10)$$

In other words, fast sodium channels instantaneously assume their steady state values following a change in membrane potential, hence adapting in a step-wise manner to a step-like change in membrane potential. Hence there is no differential equation for the Na^+ activation channels, m . This is exactly the form of the Morris-Lecar model, with the exception of a substitution of Na^+ currents with Ca^{++} . The system (4.9)–(4.10) is known as planar, as its phase space is the two-dimensional plane spanned by V (the abscissa) and n (the ordinate). To understand the dynamics we calculate the nullclines for the dynamical variables V and n . In Fig. 4.5 is

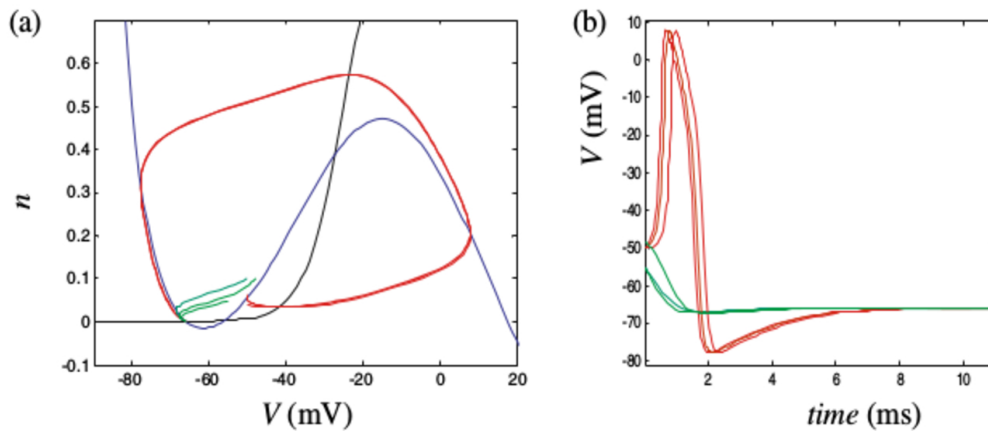


FIGURE 4.5: (a) Representative sub- (green) and supra-threshold orbits (red) and (b) their temporal evolution. The nullclines are drawn with the parameters value found in [19].

shown representative orbits of this system. Three “subthreshold” (green) and three “suprathreshold” (red) orbits are shown. In the latter case, the neuron depolarizes before returning to its resting state. It should be noted that this threshold depends not only on the initial membrane potential V but also the initial K^+ membrane conductance. The separatrix between sub- and supra-threshold is constituted by the inset of the saddle point (not shown). Whether the initial condition is sub- or supra-threshold, this system only has a single steady state solution in the current parameter regime. Hence, after at most one depolarization, it enters a quiescent state. Thereafter a discrete synaptic input, such as due to an excitatory post-synaptic potential

(EPSP), will trigger a further discharge only if it is of sufficient strength to ‘knock’ the system over the inset of the saddle point. This will hence determine whether the resulting neural response is of the green or red waveform as in Fig. 4.5.

A further examination of the equation for the V-nullcline shows that the synaptic

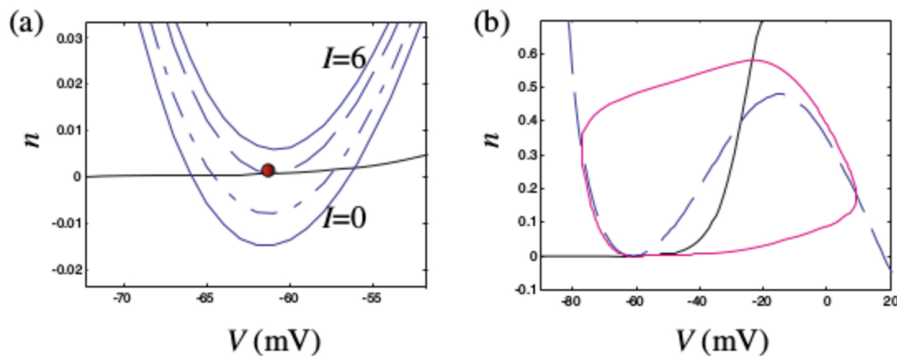


FIGURE 4.6: Saddle-node bifurcation in the planar system. (a) Nullclines near fixed points for $I = 0, 2, 4.51, 6$. Red circle denotes “saddle-node” fixed point (b) Homo-clinic orbit for the system when $I = 4.51$.

current is a purely additive term. It hence acts to translate this nullcline in the vertical direction, with no influence on its shape and no influence on the n -nullcline. In Fig. 4.6a, a close-up of the nullclines is shown for values of $I = 0, 2, 4.51$ and 6 . As I is increased from 0 to 2 (dot-dashed), we see an upward shift of the V -nullcline so that the saddle and node fixed points are closer together in phase space. At $I = 4.5$ (dashed), the nullclines are tangent and the fixed points have hence collided. At $I = 6$ (dotted) there are no nullcline intersections: hence their collision has led to their mutual annihilation. This is exactly the “saddle-node” bifurcation defined in the previous section. In the present setting, the synaptic input I functions as the bifurcation parameter. However, in addition to the structure of Fig. 4.6, an additional “global” feature of the phase space in the current system requires consideration. When the fixed points collide, the short heterocline is abolished, but the long heterocline remains (Fig. 4.5b). Indeed even when $I > 4.51$ this orbit is still an invariant of the dynamics. However, with no fixed point along its domain, it is now a continuously looping limit cycle.

Figure 4.7 shows the limit cycle attractor (red) and its temporal dynamics for $I = 4.75$ (top row) and $I = 6$ (bottom row). Note that although the phase space portraits look similar, the frequency of the dynamics increases substantially with the increase in synaptic current. This can be understood as a consequence of the bifurcation. Just after the bifurcation, although the nullclines do not intersect, the limit cycle must pass through a very narrow gap between them. The vector field in this gap bears the “memory” of the fixed points – namely it is very slow. Hence the orbits in this vicinity are near-stationary, as can be seen in the time domain. As I increases this influence diminishes and the frequency hence increases. This is the phenomenon called ghost attractor, described in section 3. Note that in both cases, however, there is virtually no change in the morphology of the depolarization, which is not related to this phenomenon. Through a slight change in the parameters relating to the potassium channels, however, the transition from steady state (fixed point) to periodic (limit cycle) dynamics can occur through a different type of bifurcation. In the above scenario the potassium channels had values consistent with a “high threshold”, namely

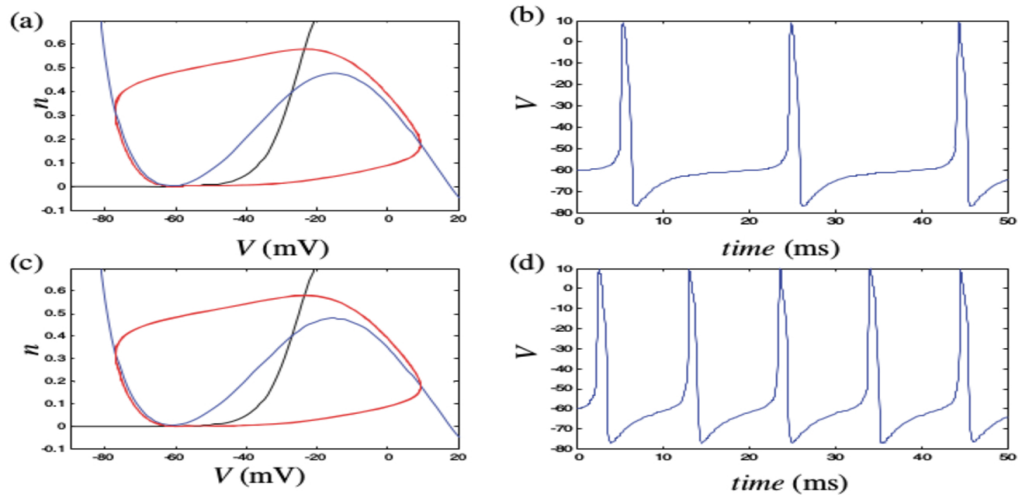


FIGURE 4.7: Limit cycle dynamics for $I=4.75$ (top row) and $I=6$ (bottom row).

the mean threshold potential of the K^+ potassium channels $V_n = -25$ mV. Lowering V_n to -45 mV and changing the Nernst potential to $V_K = -78$ mV yields the phase space portraits and time series plotted in Fig. 4.8. Firstly, there is only one intercep-

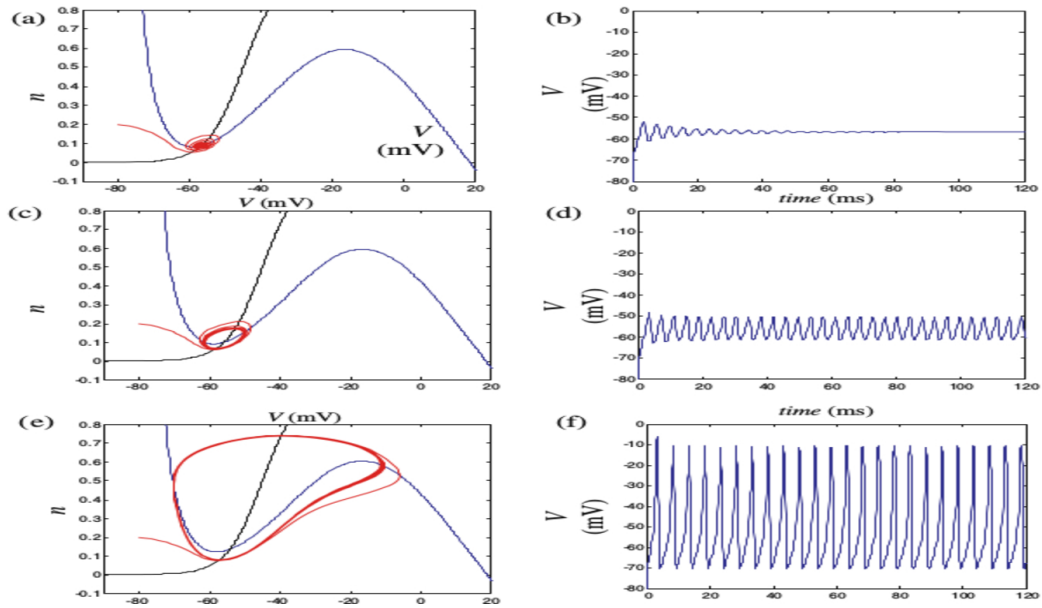


FIGURE 4.8: Phase portrait and time series of the planar model in the “low K +threshold” case for $I = 18.5$ (top row), $I = 21$ (middle row) and $I = 27$ (bottom row)

tion of the nullclines for these parameter values, and hence only one fixed point. For $I < 19$ this is a spiral inset, hence yielding damped oscillations (panels a,b). For $I > 19$ the fixed point has undergone a (supercritical) Hopf bifurcation, hence yielding a small amplitude limit cycle, coinciding with sustained but subthreshold voltage oscillations. For $I \approx 26$, the amplitude of these oscillations grows smoothly but rapidly so that with $I = 27$ the system exhibits sustained suprathreshold oscillations. However, note that the damped, subthreshold and suprathreshold oscillations all have

approximately the same frequency. This contrasts with the saddle-node scenario. We conclude with the two different bifurcation sets, Fig. 4.9, corresponding to distinct routes to sustained oscillations in this neuronal model. Panel (a) shows the saddle node bifurcation, yielding the sudden onset of suprathreshold oscillations at $I \approx 4.5$ mA. Panel (b) depicts the Hopf bifurcation with the gradual onset of sub-threshold oscillations at $I \approx 19$ mA, growing rapidly to suprathreshold with $I \approx 26$ mA. In the presence of discrete synaptic inputs, the saddle-node system will generate an all-or-nothing depolarization – or chain of depolarizations – if the input is sufficiently large. The frequency of any such chain of discharges increases with the magnitude of the synaptic input. On the other hand, the Hopf route will generate either damped, sub-threshold oscillations or a chain of depolarizations, although the frequency of these will be more or less constant. In the presence of discrete synaptic inputs, the saddle-node system will generate an all-or-nothing depolarization – or chain of depolarizations – if the input is sufficiently large.

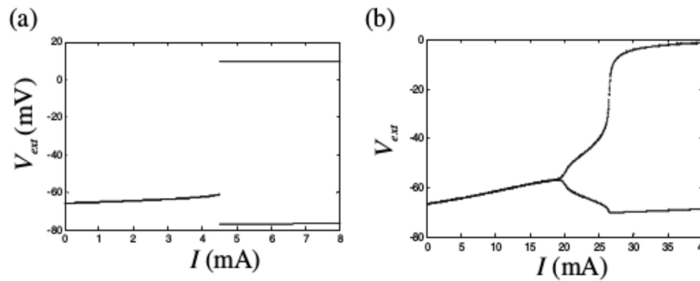


FIGURE 4.9: Saddle-node (a) and (b) Hopf bifurcation diagrams for the planar neural system with high and low K^+ channel thresholds, respectively.

As we have seen above, the shape and intersections of the nullclines plays the determining role in the behaviour and bifurcations of the dynamics. In fact, all that is required to reproduce the qualitative nature of the dynamics is the cubic-like shape of the V -nullcline and the presence of an n -nullcline with the appropriate intersections. Mathematically, these requirements can be met with the much simpler algebraic equations:

$$\begin{aligned} \frac{dx}{dt} &= x(a-x)(x-1) - y + I \\ \frac{dy}{dt} &= bx - cy \end{aligned} \quad (4.11)$$

This system - and variations of it - are known as the FitzHugh-Nagumo model and allows a closed-form analysis, with relatively simple algebraic forms, of the same qualitative phenomena as the planar model of Hodgkin-Huxley dynamics [19] and we will use these differential equations to model the neural population activity in section 5.2 when we will discuss our simulated resting state network model.

4.3 The Brain

In this paragraph it is shortly resumed the general structure of the whole brain. In particular, we will focus on the cerebral cortex, either anatomy and function, as our meso- and macro-scale model will describe this part of the brain.

The human brain is the central organ of the human nervous system, and with the spinal cord makes up the central nervous system. The brain consists of the cerebrum, the brainstem and the cerebellum. It controls most of the activities of the body, processing, integrating, and coordinating the information it receives from the sense organs, and making decisions as to the instructions sent to the rest of the body. The cerebrum is the largest part of the human brain. It is divided into two cerebral hemispheres. The cerebral cortex is an outer layer of grey matter, covering the core of white matter (see Fig. 4.10(left)). Also this region is divided into left and right cerebral hemispheres by the longitudinal fissure, but the two hemispheres are joined at the midline by the corpus callosum. Moreover, it is the largest region of the mammalian brain and plays a key role in memory, attention, perception, cognition, awareness, thought, language, and consciousness. Each hemisphere is conventionally divided into four lobes – the frontal, temporal, parietal, and occipital lobes (see Fig. 4.10(right)).

The frontal lobe is associated with executive functions including self-control, plan-

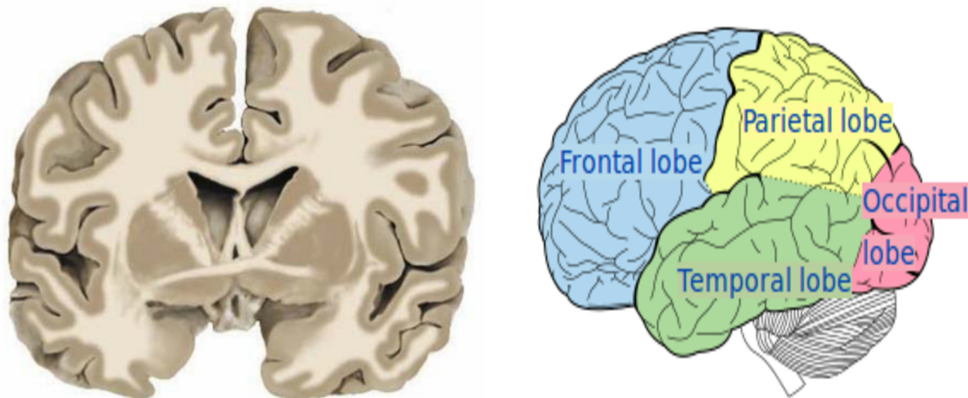


FIGURE 4.10: (left) A coronal section of the brain where the difference between white matter (light gray) and gray matter (dark gray) is visible.(right) a sketch of a human brain with the different lobes.

ning, reasoning, and abstract thought, while the occipital lobe is dedicated to vision. Within each lobe, cortical areas are associated with specific functions, such as the sensory, motor and association regions. Furthermore each different patch of the somatosensory cortex corresponds to a different body parts. Although the left and right hemispheres are broadly similar in shape and function, some functions are associated with one side, such as language in the left and visual-spatial ability in the right. At the cellular and circuit level, the cerebral cortex is characterized by two primary organizational features: 1) across its surface it is divided into functional areas that serve various sensory, motor, and cognitive functions, and 2) it is subdivided into several layers that organize the input and output connectivity of resident neurons. The different cortical layers contain a characteristic distribution of neuronal cell types and connections with other cortical and subcortical regions. The cortical

layers are not simply stacked one over the other; there exist characteristic connections between different layers and neuronal types, which span all the thickness of the cortex. These cortical microcircuits are grouped into cortical columns and minicolumns (the spacial mesoscale of the brain). These two fundamental properties provide modular functionality. Based on the differences in lamination, the cerebral cortex can be classified into two parts, the large area of neocortex and the much smaller area of allocortex. In large mammals, the cerebral cortex is usually folded, providing a greater surface area in the confined volume of the cranium. Increased surface area is thought to be important because it allows for the addition and evolution of a greater diversity of functional modules, or areas. A fold or ridge in the cortex is termed a gyrus (plural gyri) and a groove is termed a sulcus (plural sulci). In the human brain the majority of the cerebral cortex is not visible from the outside, but buried in the sulci.

Regarding the divisions of the functional area, it is important to point out two important characteristic of the brain: segregation and integration. Segregation refers to the property of some functions to be localised in certain brain areas, whereas integration involves the computation the brain performs in order to put together and elaborate information coming from different areas. How these two properties arise due to the intrinsic structure of brain is an investigated matter. At the beginning of nineteenth century, it was thought that brain was the organ of mind and that it was composed of separate areas, each being the organ of a specific behaviour; this is known as phrenology, and it was the fundamental of many psychological and psychiatric theories of the time. Although phrenology relied on some true bases, it was certainly representative of a very little part of the processes going on in the brain. Scientists started to understand that brain does not have a purely localised structure, rather all the different areas interact in order to perform more complex functions. Indeed it holds true that simpler functions refer to specific areas within the brain. Thus we can talk about more localised structures dedicated to simpler functions, as the sensory cortices (visual cortex, auditory cortex, somatosensory cortex) and the motor cortex. However association areas are responsible for performing more complex operations or for emotions. Nevertheless, the most common neuroscientific way of thinking about brain mechanisms is in term of connections or interactions between different specialised areas. With this viewpoint, then, an area is specialised to a given function rather than to another because neurons in that area are connected, cooperate and activate together. However connections are present among very different parts: an example is carried by the high number of axon fibres connected cortical neurons among the two hemispheres. Nevertheless it has to be noted that brain connections are not static and determined once and for all. Synapses can be formed and deleted in various ways and these processes are thought to be the underlying neurobiological bases from which the concept of memory arises.

4.4 Population dynamics

The goal of any large-scale description of neural dynamics is to reconstruct all relevant spatiotemporal dynamics of the neural system while preserving the mechanism which give rise to the observed dynamics. The assumption behind large scale models is that the neurocomputational units are more macroscopic than a single neuron. This assumption is justified by the fact that the key features of brain operations seem to emerge from the component interplay rather than being generated by each individual component. Large scale models are the instruments to interpret the enormous

data sets obtained from non-invasive brain imaging. Moreover large scale models are easier and less time-consuming to be solved computationally; actually today the the current technology allows to implement simulations of network with size significantly smaller than the amount of neurons we have in our brain. In this paragraph it is briefly summarized the mathematical steps which permit the description of the large scale models in the general case of homogeneous population of integrate-and-fire neurons. For an exhaustive discussion about this topic we refer to [25].

In many areas of the brain neurons are organized in populations of units with similar properties. Prominent examples are columns in the somatosensory and visual cortex and pools of motor neurons . Given the large number of neurons within such a column or pool it is sensible to describe the mean activity of the neuronal population rather than the spiking of individual neurons. In a population of N neurons, we calculate the proportion of active neurons by counting the number of spikes $n_{act}(t;t+\Delta t)$ in a small time interval Δt and dividing by N . Further division by Δt yields the population activity

$$A(t) = \lim_{\Delta t \rightarrow 0} \frac{1}{\Delta t} \frac{(n_{act}(t;t + \Delta t))}{N} = \frac{1}{N} \sum_{j=0}^N \sum_{f=0}^M \delta(t - t_j^{(f)}) \quad (4.12)$$

where δ denotes the Dirac δ function. The double sum runs over all firing times $t_j^{(f)}$ of all neurons in the population. In other words the activity A is defined by a population average. We study a large and homogeneous population of neurons. By homogeneous we mean that all neurons $1 \leq i \leq N$ are identical and receive the same external input $I_{i,ext}(t) = I_{ext}(t)$. Moreover, in a homogeneous population, the interaction strength between the neurons is taken to be uniform,

$$w_{ij} = \frac{J_0}{N} \quad (4.13)$$

where J_0 is a parameter. For $J_0 = 0$ all neurons are independent; a value $J_0 > 0$ ($J_0 < 0$) implies excitatory (inhibitory) all-to-all coupling. The interaction strength scales with one over the number of neurons so that the total synaptic input to each neuron remains finite in the limit of $N \rightarrow \infty$. Model neurons are described by formal spiking neurons and for the sake of simplicity we consider the leaky integrate-and-fire neurons with

$$\tau_m \frac{du_i}{dt} = -u_i + RI_i(t) \quad (4.14)$$

An homogeneous network implies that all neurons have the same input resistance R , the same membrane time constant τ_m , as well as identical threshold and reset values. The input current I_i takes care of both the external drive and synaptic coupling

$$I_i = \sum_{j=0}^N \sum_{f=0}^M w_{ij} \alpha(t - t_j^{(f)}) + I^{ext}(t) \quad (4.15)$$

Here we have assumed that each input spike generates a postsynaptic current with some generic time course $\alpha(t - t_j^{(f)})$. The sum on the right-hand side of (4.15) runs over all firing times of all neurons. Because of the homogeneous all-to-all coupling, the total input current is identical for all neurons. To see this, we insert Eq. (4.14) and use the definition of the population activity, Eq. (4.13). We find a total input

current,

$$I(t) = J_0 \int_0^\infty \alpha(s) A(t-s) ds + I^{ext}(t) \quad (4.16)$$

which is independent of the neuronal index i . As an aside we note that for conductance-based synaptic input, the total input current would depend on the neuronal membrane potential which is different from one neuron to the next. In the absence of noise, the next firing time of a spiking neuron i is found from the threshold condition,

$$u_i(t) = \theta \text{ and } \frac{du_i}{dt} > 0 \quad (4.17)$$

Instead, in the presence of noise, the next firing time of a given neuron i cannot be predicted in a deterministic fashion. In the case of integrate-and-fire neurons with diffusive noise (stochastic spike arrival), a large noise level leads to a broad distribution of the membrane potential and indirectly to a large distribution of interspike intervals. In the case of spiking neurons with escape noise (noisy threshold), firing occurs probabilistically which results in a similar large distribution of interspike intervals.

In a population of neurons, each neuron may be in a different internal state. Now we derive partial differential equations that describe how the distribution of internal states evolves as a function of time, that is, we describe the dynamics of the population as the evolution of membrane potential densities. In a population of N integrate-and-fire neurons, we may ask how many of the neurons have at time t a given membrane potential. For $N \rightarrow \infty$ the fraction of neurons i with membrane potential $u_0 < u_i(t) \leq u_0 + \Delta u$ is

$$\lim_{N \rightarrow \infty} \frac{\text{neurons with } u_0 < u_i(t) \leq u_0 + \Delta u}{N} = \int_{u_0}^{u_0 + \Delta u} p(u, t) du \quad (4.18)$$

where $p(u, t)$ is the membrane potential density. The integral over the density remains constant over time, i.e.,

$$\int_{-\infty}^{\theta} p(u, t) du = 1 \quad (4.19)$$

The normalization to unity expresses the fact that all neurons have a membrane potential below or equal to threshold. Then, the fraction of neurons that ‘flow’ across threshold per unit of time is the (expected value of) the population activity $A(t)$. If we denote the flux across threshold as $J(\theta, t)$, we have

$$A(t) = J(\theta, t) \quad (4.20)$$

Due to the reset, the neurons that ‘disappear’ across threshold, ‘reenter’ at the reset potential u_r . Hence, the membrane potential density at $u=u_r$ increases at a rate proportional to $A(t)$. More specifically, we have a ‘source’ term $A(t)\delta(u - u_r)$ at the reset potential u_r that balances the loss that is due to the movement across the threshold. We assume that all neurons in the population receive the same driving current I_{ext} . In addition each neuron receives stochastic background input. We allow for different types of synapse. An input spike at a synapse of type k causes a jump of the membrane potential by an amount w_k . The effective spike arrival rate (summed over all synapses of type k) is denoted as ν_k . While the mean spike arrival rates $\nu_k(t)$ are identical for all neurons, we assume that the actual input spike trains at different neurons and different synapses are independent. With these assumptions, the

dynamics for $u \leq \theta$ is

$$\begin{aligned} \frac{\partial p(u, t)}{\partial t} = & \frac{p(u, t)}{\tau_m} - \frac{1}{\tau_m} [-u + RI^{ext}(t)] \frac{\partial p(u, t)}{\partial u} + \\ & + \sum_{k=0}^N v_k(t) [p(u - w_k, t) - p(u, t)] + A(t) \delta(u - u_r) \end{aligned} \quad (4.21)$$

The first two terms on the right-hand side describe the continuous drift, the third term the jumps caused by stochastic spike arrival, and the last term describes the reset. Because of the firing condition, we have $p(u, t) = 0$ or $u > \theta$. In order to calculate the population activity $A(t)$, we need to determine the flux across threshold. To keep the argument slightly more general, we will consider the flux $J(u_0, t)$ across an arbitrary reference potential u_0 ,

$$J(u_0, t) = J_{drift}(u_0, t) + J_{jump}(u_0, t) \quad (4.22)$$

where J_{drift} accounts for the continuous drift of the membrane potential during the time when no input spike arrives. J_{jump} is due to excitatory and inhibitory spike arrival. To evaluate J_{jump} , let us consider excitatory input $w_k > 0$ first. All neurons that have a membrane potential u_i with $u_0 - w_k < u_i \leq u_0$ will jump across the reference potential u_0 upon spike arrival at synapse k . Since the rate of spike arrival at synapse k is v_k , the total flux caused by input spikes at all synapses is

$$J_{jump}(u_0, t) = \sum_{k=0}^N v_k \int_{u_0 - w_k}^{u_0} p(u, t) du \quad (4.23)$$

The drift $J_{drift}(u_0, t)$ through the reference potential u_0 is given by the density $p(u_0, t)$ at the potential u_0 times the momentary ‘velocity’ du/dt . With $du/dt = [-u + RI^{ext}(t)]/\tau_m$ we have

$$J_{drift}(u_0, t) = -\frac{1}{\tau_m} [-u_0 + RI^{ext}(t)] p(u_0, t) \quad (4.24)$$

The total flux at the threshold $u_0 = \theta$ yields the population activity

$$A(t) = \frac{1}{\tau_m} [-\theta + RI^{ext}(t)] p(\theta, t) + \sum_{k=0}^N v_k \int_{\theta - w_k}^{\theta} p(u, t) du \quad (4.25)$$

Since the probability density vanishes for $u > \theta$, the sum over the synapses k can be restricted to all excitatory synapses. Eqs. (4.22) and (4.26) define the dynamics in a population of integrate-and-fire neurons with stochastic background input. In the limit of small jump amplitudes w_k , the density dynamics (4.22) can be approximated by a diffusion equation. To show this we expand the right-hand side of Eq. (4.22) into a Taylor series up to second order in w_k . The result is the Fokker-Planck equation,

$$\begin{aligned} \tau_m \frac{\partial p(u, t)}{\partial t} = & -\frac{\partial [-u + RI^{ext}(t) + \tau_m \sum_{k=0}^N v_k(t) w_k] p(u, t)}{\partial u} + \\ & \frac{1}{2} \tau_m \sum_{k=0}^N v_k(t) w_k^2 \frac{\partial^2 p(u, t)}{\partial u^2} + \tau_m A(t) \delta(u - u_r) + O(w_k^3) \end{aligned} \quad (4.26)$$

The term with the second derivative describes a ‘diffusion’ in terms of the membrane potential. The firing threshold acts as an absorbing boundary so that the density at

threshold vanishes, $p(\theta, t) = 0$. In order to calculate the flux through the threshold we expand Eq. (4.26) in w_k about $u = \theta$ and obtain

$$A(t) = -\frac{\sigma^2(t)}{2\tau_m} \frac{\partial p(u, t)}{\partial u} \Big|_{u=\theta} \quad (4.27)$$

where we have defined

$$\sigma^2(t) = \tau_m \sum_{k=0}^N v_k(t) w_k^2 \quad (4.28)$$

Eqs. (4.26) – (4.27) together with the normalization define the dynamics of a homogeneous population of integrate-and-fire units with ‘diffusive’ noise.

Now we derive the stationary solution $p(u, t) \equiv p(u)$ of the Fokker-Planck equation (4.26). The stationary distribution $p(u)$ of the membrane potential is of particular interest, since it is experimentally accessible. We assume that the total input $h_0 = RI^{ext} + \tau_m \sum_{k=0}^N v_k w_k$ is constant. In the stationary state, the temporal derivative on the left-hand-side of Eq. (4.26) vanishes. The terms on the right-hand side can be transformed so that the stationary Fokker-Planck equation reads

$$0 = -\frac{\partial J(u)}{\partial u} + A_0 \delta(u - u_r) \quad (4.29)$$

where A_0 is the population activity (or mean firing rate) in the stationary state and

$$J(u) = \frac{-u + h_0}{\tau_m} p(u) - \frac{\sigma^2}{2\tau_m} \frac{\partial p(u)}{\partial u} \quad (4.30)$$

is the total flux. The meaning of Eq. (4.30) is that the flux is constant except at $u = u_r$ where it jumps by an amount A_0 . Similarly, the boundary condition $p(\theta, t) = 0$ implies a second discontinuity of the flux at $u = \theta$. We expect that the stationary solution approaches a Gaussian distribution for $u \rightarrow -\infty$. In fact, we can check easily that for any constant c_1 :

$$p(u) = \frac{c_1}{\sigma} \exp\left[-\frac{(u - h_0)^2}{\sigma^2}\right] \text{ for } u \leq u_r \quad (4.31)$$

is a solution of Eq. (4.30) with flux $J(u) = 0$. However, for $u > u_r$ a simple Gaussian distribution cannot be a solution since it does not respect the boundary condition $p(\theta) = 0$. Nevertheless, we can make an educated guess and try a modified Gaussian,

$$p(u) = \frac{c_2}{\sigma^2} \exp\left[-\frac{(u - h_0)^2}{\sigma^2}\right] \int_u^\theta \exp\left[-\frac{(x - h_0)^2}{\sigma^2}\right] dx \text{ for } u_r < u \leq \theta \quad (4.32)$$

with some constant c_2 . We have written the above expression as a product of two terms. The first factor on the right-hand side is a standard Gaussian while the second factor guarantees that $p(u) \rightarrow 0$ for $u \rightarrow \theta$. If we insert Eq. (4.32) in (4.29) we can check that it is indeed a solution. The constant c_2 is proportional to the flux,

$$c_2 = 2\tau_m J(u) \text{ for } u_r < u \leq \theta \quad (4.33)$$

The solution defined by Eqs. (4.32) and (4.33) must be continuous at $u = u_r$. Hence

$$c_1 = \frac{c_2}{\sigma} \int_{u_r}^\theta \exp\left[-\frac{(x - h_0)^2}{\sigma^2}\right] dx \quad (4.34)$$

Finally, the constant c_2 is determined by the normalization condition:

$$\frac{1}{c_2} = \int_{-\infty}^{\theta} \int_{u_r}^{\theta} f(x, u) dx du + \int_{u_r}^{\theta} \int_u^{\theta} f(x, u) dx du = \int_{u_r}^{\theta} \int_{-\infty}^x f(x, u) du dx \quad (4.35)$$

with

$$f(x, u) = \frac{1}{\sigma^2} \exp\left[-\frac{(u - h_0)^2}{\sigma^2}\right] \exp\left[\frac{(x - h_0)^2}{\sigma^2}\right] \quad (4.36)$$

The activity A_0 is identical to the flux $J(u)$ between u_r and θ and therefore proportional to the constant c_2 ; cfr. Eq. (4.34). If we express the integral over u in (4.36) in terms of the error function, $\text{erf}(x)$, we obtain

$$A_0^{-1} = \tau_m \sqrt{\pi} \int_{\frac{u_r - h_0}{\sigma}}^{\frac{\theta - h_0}{\sigma}} \exp(x^2) [1 + \text{erf}(x)] dx \quad (4.37)$$

The stationary dynamics of each population can be described by the population transfer function of Ricciardi ϕ (where $\phi(\mu, \sigma) = A_0$), which provides the average population rate as a function of the average input current. The result found in equation 4.37 can be generalized for more than one population of neurons whose input currents share the same statistical properties and fire spikes independently at the same rate:

$$r_i = \phi(\mu_i, \sigma_i) \quad (4.38)$$

To solve equation 4.38 for all the neural population i , the differential equation below can be integrated while it describes the approximate dynamics of the system which has a fixed point solutions corresponding to equation 4.38:

$$\tau_i \frac{dr_i}{dt} = -r_i + \phi(\mu_i, \sigma_i) \quad (4.39)$$

The mean field approach ensures that this dynamics will converge to a stationary attractor that is consistent with the steady state required. In the next section an extended mean field framework will be analyzed. This model is consistent with the LIF model and with the realistic synaptic equations of Hodgkin-Huxley model.

Chapter 5

Materials and Methods

From this chapter start the real core of the thesis because it is illustrated the materials and the methods used to simulate and analyse the resting state network activity.

The first section contains information about the innovative software used to implement the simulation, The Virtual Brain (TVB), giving a brief overview of its functionality and the reason of its importance in computational neuroscience.

Secondly, the network model for the computation of the resting state dynamic is described, starting from the large-scale network connectivity until the meso-scale dynamics of the neuron mean field used to simulate the nodes of the network.

Finally, the simulation set-up is illustrated, explaining how we choosed the parameter values and the procedure followed for the numerical computation and analysis.

5.1 The Virtual Brain

We present The Virtual Brain (TVB), a neuroinformatics platform for full brain network simulations using biologically realistic connectivity. This simulation environment enables the model-based inference of neurophysiological mechanisms across different brain scales that underlie the generation of macroscopic neuroimaging signals including fMRI, EEG and MEG. Researchers from different backgrounds can benefit from an integrative software platform including a supporting framework for data management (generation, organization, storage, integration and sharing) and a simulation core written in Python.

TVB allows the reproduction and evaluation of personalized configurations of the brain by using individual subject data. This personalization facilitates an exploration of the consequences of pathological changes in the system, permitting to investigate potential ways to counteract such unfavourable processes.

Brain function is thought to emerge from the interaction of large numbers of neurons, under the spatial and temporal constraints of brain structure and cognitive demands. Contemporary network simulations mainly focus on the microscopic and mesoscopic level (neural networks and neural masses representing a particular cortical region), adding detailed biophysical information at these levels of description while too often losing perspective on the global dynamics of the brain. On the other hand, the degree of assessment of global cortical dynamics, across imaging modalities, in human patients and research subjects has increased significantly in the last few decades. Hence, TVB response to the need of developing an efficient, flexible, neuroinformatics platform on this macroscopic level of brain organization for reproducing and probing the broad repertoire of brain dynamics, enabling quick data analysis and visualization of the results. It provides a general infrastructure to support multiple users handling various kinds of empirical and simulated data, as well as tools for visualizing and analysing that data, either via internal mechanisms or by interacting with other computational systems.

At the same time it provides a simulation toolkit to support a top-down modelling approach to whole brain dynamics, where the underlying network is defined by its structural large-scale connectivity and mesoscopic models that govern the nodes' intrinsic dynamics. The interaction with the dynamics of all other network nodes happens through the connectivity matrix via specific connection weights and time delays. Thus the simulation side of TVB has evolved out of a research program seeking to identify and reproduce realistic whole brain network dynamics, on the basis of empirical connectivity and neural field models [11].

5.2 The Resting State Network model

When traversing the scale to the large-scale network, then each network node is governed by its own intrinsic dynamics in interaction with the dynamics of all other network nodes. This interaction happens through the connectivity matrix via specific connection weights and time delays due to signal transmission delays. The following (generic) evolution equation captures all the above features and underlies the emergence of the spatiotemporal network dynamics in TVB:

$$\begin{aligned} \dot{\Psi}(x, t) = & N(\Psi(x, t)) + \int_{\Gamma} g_{local}(x, x') S(\Psi(x', t)) dx' + \\ & \int_{\Gamma} g_{global}(x, x') S(\Psi(x', t - \frac{|x - x'|}{v})) dx' + I(x, t) + \zeta(x, t) \end{aligned} \quad (5.1)$$

The equation describes the stochastic differential equation of a network of connected neural populations. $\Psi(x, t)$ is the neural population activity vector at the location x in 3D physical space and time point t . It has as many state variables as are defined by the neural population model, which is specified by $N(\Psi(x, t))$. The connectivity distinguishes local and global connections, which are captured separately in two expressions. The local network connectivity $g_{local}(x, x')$ is described by connection weights between x and x' , whereas global connectivity is defined by $g_{global}(x, x')$. The critical difference between the two types of connectivity is threefold:

- Local connectivity is short range (order of cm) and global connectivity is long range (order of tens of cm).
- Signal transmission via local connections is instantaneous, but via global connections undergoes a time delay dependent on the distance $|x - x'|$ and the transmission speed v .
- Local connectivity is typically spatially invariant (of course with variations from area to area, but generally it falls off with distance), global connectivity is highly heterogeneous.

Therefore, two types of structural connectivity are distinguished in TVB, that is long- and short-range connectivity, given by the connectivity matrix and the folded cortical surface, respectively. However, we are not taking in account the surface-based model. Stimuli of any form, such as perceptual, cognitive or behavioural perturbations, are introduced into the virtual brain via the expression $I(x, t)$ and are defined over a location x with a particular time course. As we are studying the resting state network dynamics, we will neglect also this component. We will see that noise plays a crucial role for the brain dynamics and hence for brain function. In TVB it is introduced via the expression $\zeta(x, t)$ where the type of noise and its spatial and temporal correlations can be specified independently.

At the local level of a brain area, the simplest assumption is to consider a network of interacting spiking neurons that are organized into a discrete set of populations. Populations are defined as groups of statistically similar excitable neurons that share the same inputs and connectivity. A spiking neuron transforms a large set of incoming input spike trains from different neurons into an output spike train. Thus, at the microscopic level, neuronal circuits of the brain encode and process information through spatiotemporal spike patterns. In the brain, local neuronal networks comprise a large number of neurons that are massively interconnected. The dynamics can be properly described by a set of coupled differential equations corresponding to a model for each neuron. One way to overcome these difficulties is by adopting the population density approach, using the Fokker–Planck formalism. In this approach, individual integrate-and-fire neurons are grouped together into populations of statistically similar neurons (cfr. Section 4.4). Assuming the population density approach, we can reduce the description of the dynamics of a local circuit by using the mean-field equations that describe the evolution of the population activity of neurons pool. The simplest mathematical model that is still capable describe a lot of neural dynamic is the FitzHugh-Nagumo model [23]. The model consists of

- a voltage-like variable having cubic nonlinearity that allows regenerative self-excitation via a positive feedback,
- a recovery variable having a linear dynamics that provides a slower negative feedback.

The model is sometimes written in the abstract form:

$$\begin{aligned}\dot{V} &= d\tau(-fV^3 + eV^2 + gV + \alpha W + \gamma I) \\ \dot{W} &= \frac{d}{\tau}(cV^2 + bV - \beta W + a)\end{aligned}\quad (5.2)$$

The result had a stable resting state, from which it could be excited by a sufficiently large electrical stimulus to produce an impulse. A large enough constant current stimulus produced a train of impulses. These equations were similar to those describing the electronic circuit called a monostable multivibrator. At about the same time, an electronic circuit was built by the Japanese engineer Jin-Ichi Nagumo, using tunnel (Esaki) diodes (see Fig 5.1).

FitzHugh modified the van der Pol model for the nonlinear relaxation oscillator

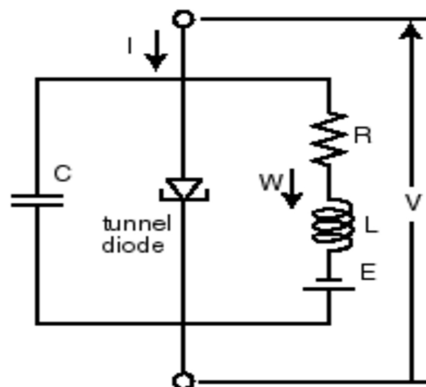


FIGURE 5.1: Nagumo circuit.

to explain the basic properties of excitability as exhibited by the more complex HH equations. The nullclines of the van der Pol equation are a vertical line and a cubic that intersect in a single rest point which is always unstable. In order to resemble a real nerve, this new model should also have only one restpoint, now basically stable, and display a threshold phenomenon for a parameter change that preferably should look like 'current stimulation'. The dynamic equations of this model are composed of two ordinary differential equations comprising two nullclines (Fig. 5.2). The first nullcline is a cubic function as it is found in most neuron and population models; the second nullcline is arbitrarily configurable as a polynomial function up to second order. The manipulation of the latter nullcline's parameters allows to generate a wide range of different behaviours. The motivation for the FitzHugh-Nagumo model was to isolate conceptually the essentially mathematical properties of excitation and propagation from the electrochemical properties of sodium and potassium ion flow. While the Hodgkin-Huxley Model is more biophysically realistic, only projections of its four-dimensional phase trajectories can be observed. The simplicity of the FitzHugh-Nagumo model permits the entire solution to be viewed at once. This allows a geometrical explanation of important biological phenomena related to neuronal excitability and spike-generating mechanism. The intersection of nullclines is an equilibrium (because $\dot{V} = \dot{W} = 0$), which may be unstable if it is on the middle branch of the V-nullcline, i.e., when I is strong enough. In this case, the model exhibits periodic (tonic spiking) activity. Recent advances in neural mass models have rediscovered the mathematical structure of the Fitz-Hugh Nagumo model as a good representation of neural population activity, as in [24]. In this sense, the mathematical structure of the planar FitzHugh-Nagumo model serves here as the intrinsic dynamics of any given network node [10] and it is choosed to show that a lot of interesting properties arise even with a simple mathematical representation, underlying in this way the importance of the connectivity between the nodes.

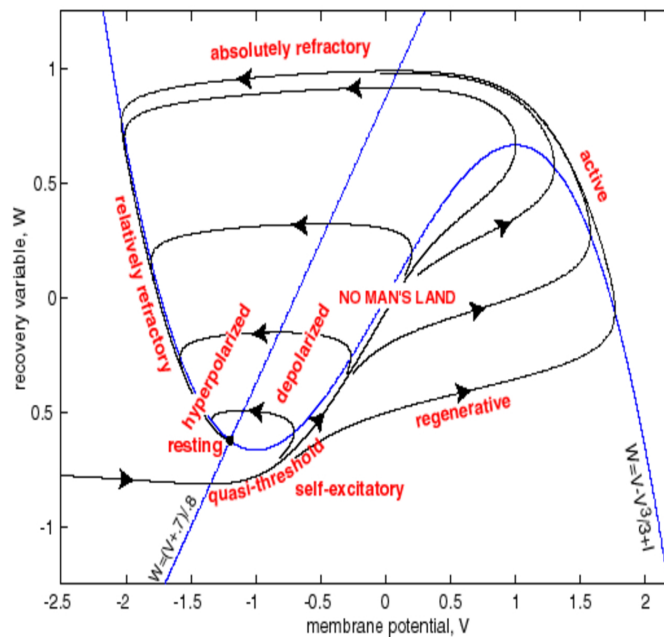


FIGURE 5.2: Phase portrait and physiological state diagram of FitzHugh-Nagumo model [23].

Parameter	a	b	c	d	e	f	g	I	alpha	beta	gamma	tau
Value	1.05	-1.0	0	0.1	0	1/3	1	0	1	0.2	-1	1.25

TABLE 5.1: The parameters value taken from [8] and [10] which reproduce the limit cycle behaviour.

5.3 Simulation Set-up

A basic simulation of discrete brain network model, as described in the previous section, consists of five main components, each of these components is a configurable object in TVB:

- Local population model, which is, at its core, a set of differential equations describing the local neuronal dynamics, and we choose the FitzHugh-Nagumo Model. The parameters values are shown in table 5.1.
- Connectivity, represents the large scale structural connectivity of the brain, ie, white-matter tracts, which is described below;
- Long range coupling, is a function that is used to join the local dynamics at distinct locations over the connections described in the connectivity. In this work it is used a linear coupling model.
- Integrator, is the integration scheme that will be applied to the coupled set of differential equations; we use the Heun methods either deterministic and stochastic in order to illustrate the role of the noise. The most important thing here is to use a step size that is small enough for the integration to be numerically stable. Here, we chose a value of $dt = 0.1$ ms. Then, we provide the simulation length. Here we use the default value of 1000 ms (2000 ms for the parameter search).
- Monitors, one or more monitors can be attached to a simulation, they act to record the output data instantaneously after the simulation's end (e.g. Time series). Moreover, the Temporal Average monitor averages over a time window of length sampling period returning one time point every period. In our simulations the monitor's sampling period is 1 ms.

One of the most important step is to determine the structural connectivity. We choose to leave the default connectivity (see Fig 5.2 and 5.3). TVB incorporates a biologically realistic, large-scale connectivity of brain regions in the primate brain. Connectivity is mediated by long-range neural fiber tracts as identified by tractography based methods or obtained from CoCoMac neuroinformatics database and subcortical regions (e.g. thalamus and other subcortical nuclei) are not included in this matrix. In TVB, the tract-lengths matrix of the demonstration connectivity dataset is symmetric due to the fiber detection techniques used to extract the information being insensitive to directionality. On the other hand, the weights matrix is asymmetric as it makes use of directional information contained in the tracer studies of the CoCoMac database. In the following bullet list the major features are summarized:

- The parcellation (connectome of 66 regions) was chosen to be as homologous as possible between Macaque and Human.

Chapter 6

Results and discussion

In this chapter is summarized the results obtain in the simulation with TVB, showing the most striking outcome of the computational study of our resting state network. Then other similar works on resting state are illustrated in order to compare our analysis with the recent researches in neuroscience. In particular it is discussed the most peculiar characteristic found in the ongoing mental dynamic, such as the role of noise, time delay and criticality.

Finally, some of the future goal in this studies, like the clinical application that will derive from a full understanding of the intrinsic mental activity and the importance of simulate brain disease, are discussed.

6.1 Analysis results

First of all, we checked the phase plane of the FitzHugh-Nagumo model with the parameter of the table 5.1 and, as we expected, we obtain a typical oscillator behaviour (Fig. 6.1) as it clearly shows a limit cycle. We tested the attractor with many different initial condition (in the figure correspond with the orbit with different colours).

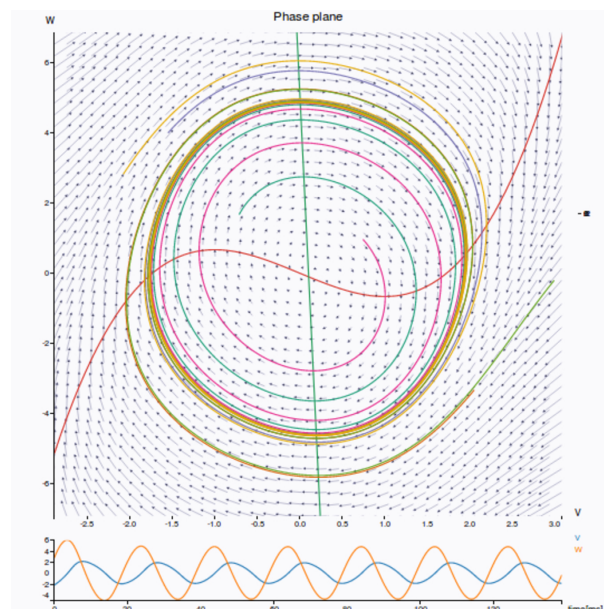


FIGURE 6.1: Phase plane and time series of the FitzHugh-Nagumo model with the parameter in table 5.1 with several orbits start from different initial conditions.

Then, using the same parameter values for simulate the network nodes, we first set

up a parameter search in order to find the best values for the long range connectivity parameter (coupling and time delay given by the conduction speed) by defining a range of values that will be explored. We set the long range coupling function in the range between 0.012 and 0.042 and the step to 0.002 and conduction speed, setting the range between 1-10 and the step to 1 mm/ms. Then we set the simulation length to 2000 ms and we launch the simulations. The results of this parameter exploration

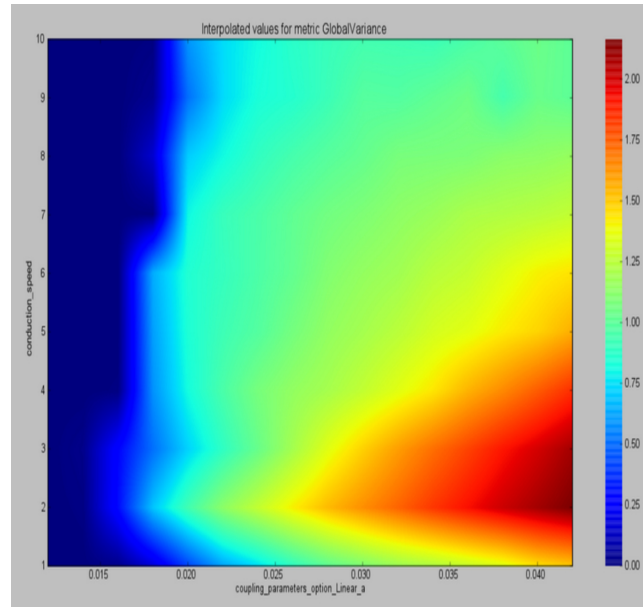


FIGURE 6.2: Continuous pseudocolor map of the parameter search with the parameter control the strength coupling and the conduction speed where the different colours show the global variance.

is illustrated in the Fig 6.2, where the different colour in the pseudo-map indicate the value of the global variance. We noted a clear area in the low right part of the graph with the higher values of the variance. Thus, we find the correct parameters in the red area of the Fig. 6.2, where the system is near the bifurcation between the stability and the oscillatory behaviour. From the researches we aware of [15], we know that the best correlation with the experimental data is in this critical region. Hence, we choose the value 0.042 for the coupling strength and 4 mm/ms for the conduction speed in order to permit system exhibits self-sustained oscillations, with the frequency peak between 10^{-2} and 10^{-1} Hz (fig 6.3). Afterwards, we also calculate the cross correlation of the nodes and the results is showed below in Fig 6.4, where it is already possible to see some clustering property. However, it is still far from the cross correlation found in literature we aware of. This means that something is missing in our resting state model.

Therefore, as a last point, we show a simulation driven by noise (i.e., using a stochastic integration scheme). In a stochastic integration scheme noise enters through the integration scheme. Here we define a simple constant level of noise that enters all nodes and all state variables. The noise functions are fed by a random process generated by a pseudo-random number generator (PRNG). The random process is defined using two parameters plus the seed of the PRNG (set at 42). The two parameters are:

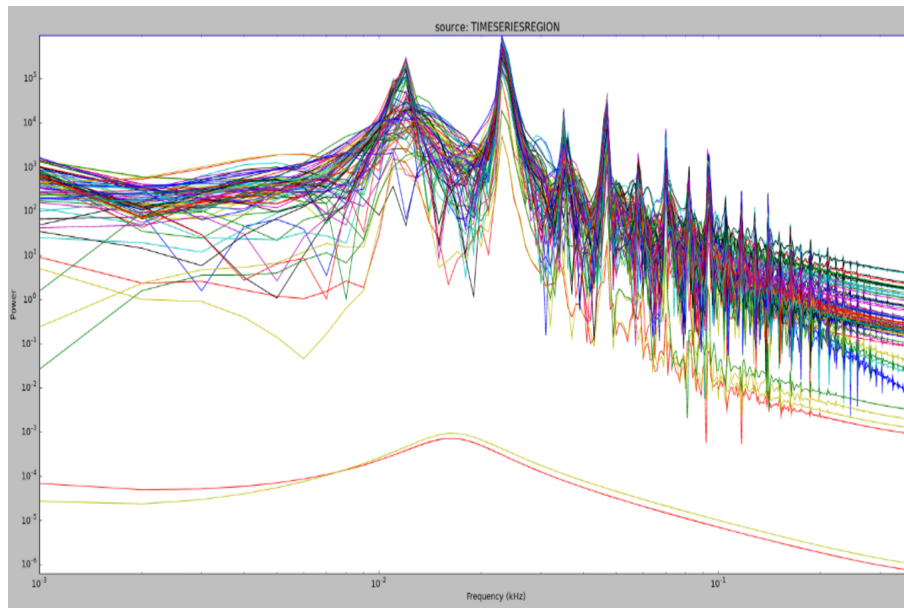


FIGURE 6.3: Fourier analysis of the frequency time series without noise (log-log scale).

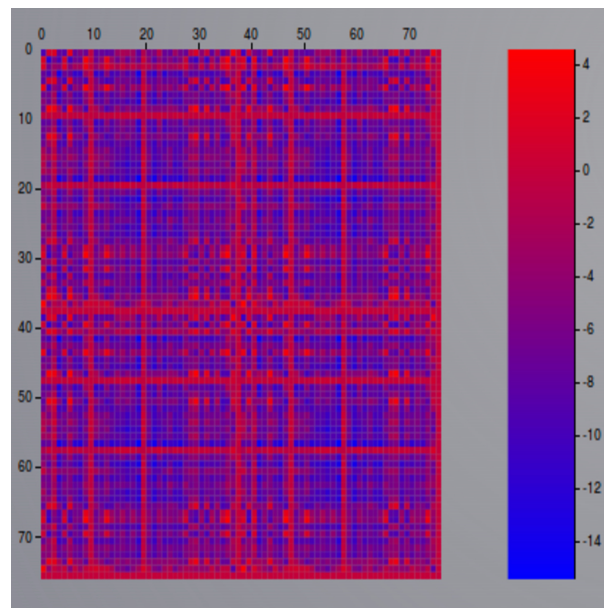


FIGURE 6.4: Cross correlation matrix of the nodes, without noise.

- D , set at 0.005, defining the standard deviation of the noise amplitude;
- τ which defines the correlation time of the noise source, with $\tau=0$ corresponding to white noise and any value greater than zero producing coloured noise.

We compute again the Fourier analysis of the frequencies and we obtain that the peak is almost the same than the one without noise, as it is illustrated in Fig. 6.5. Finally we draw the matrix of the cross correlation of nodes; in this case the matrix is quite different from the first one, as the clustering property and the anti-correlation now is more evident (Fig. 6.6) and it is more similar at the matrices obtained by

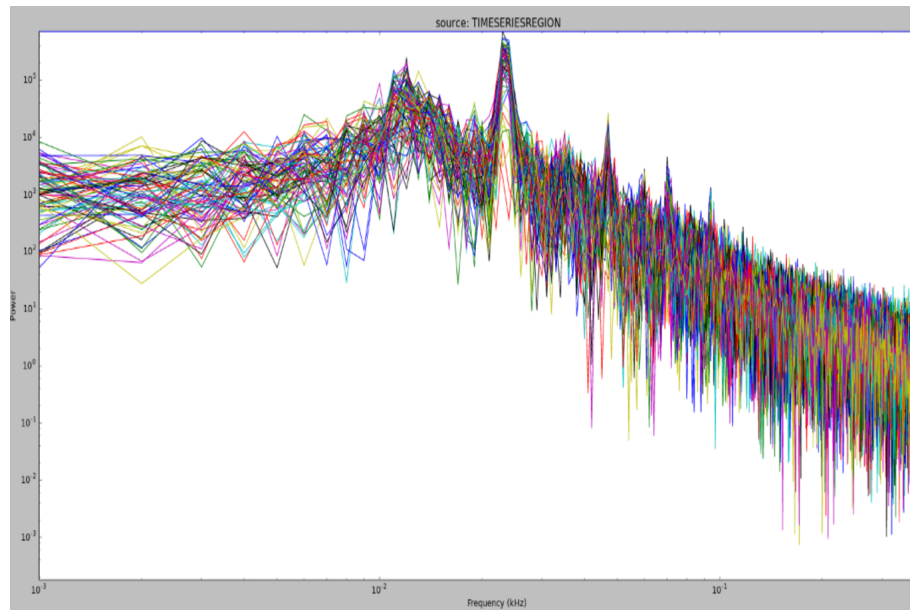


FIGURE 6.5: Fourier analysis of the frequency time series with noise (log-log scale).

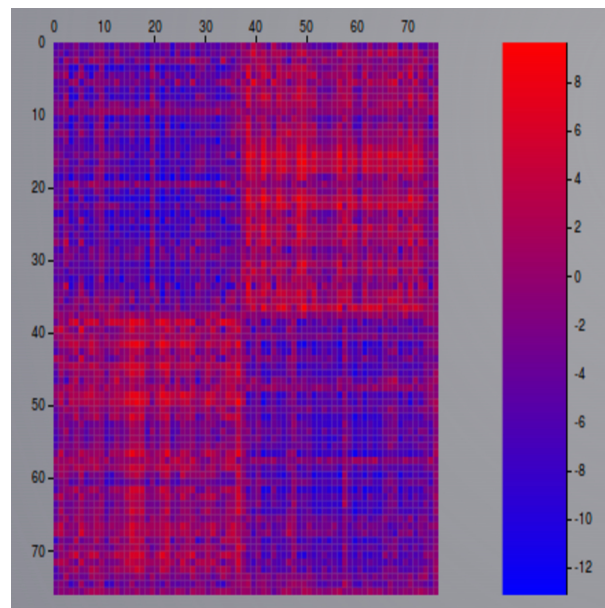


FIGURE 6.6: Cross correlation matrix of the nodes, with noise.

experimental time series data. In addition, the matrix in Fig 6.6 looks more like the structural connectivity matrix in Fig. 5.4 than that one in Fig 6.4.

6.2 Comparison with the literature

Also Deco et al. in [6] studied the dynamics of a simplified cortical network using 38 noise-driven Wilson–Cowan oscillators [26], which in isolation remain just below their oscillatory threshold. They found that time delay coupling based on lengths and strengths of primate cortico-cortical pathways leads to the emergence of 2 sets of 40-Hz oscillators. The sets showed synchronization that was anticorrelated at <0.1 Hz across the sets in line with a wide range of recent experimental observations. An additional finding in [6] was that the optimal noise level had a characteristic scale, indicating the presence of stochastic resonance, which allows the network dynamics to respond with high sensitivity to changes in diffuse feedback activity. The authors believe that the particular dynamics of the intrinsic properties of the brain are useful for keeping the system in a high competition state between the different subnetworks that later are used during different tasks. In this way, a relatively small external stimulation is able to stabilize one or the other subnetwork giving rise to the respective evoked activity. In this way, an active resting state (fluctuating between multistable states) can be sensitive to external signals that can trigger the activation of one of several available multistable states. This extends to the level of global dynamics a principle that was demonstrated at the level of local dynamics, where the competitive balance between excitation and inhibition ensures the emergence of unified network states that are important for local processing in attention, memory, and decision making.

Moreover, the role of noise in brain activity was studied also in [7] where the authors showed that neuronal networks that have formed in the presence of noise will be more robust and explore more states, which will facilitate learning and adaptation to the changing demands of a dynamic environment (Fig. 6.7). The presence of noise in nervous systems has profound implications for their computational power. Yet, despite significant noise levels our brain appears to function reliably, presumably because it has evolved under the constraints that are imposed by noise. Therefore, to understand the nervous system we have to distinguish variability from noise by accounting for its sources and appreciate the way in which it influences the brain's structure and function. The ongoing interplay between noise drive and oscillatory return leads to the exploration of the brain's dynamics repertoire. The latter repertoire spans temporal scales of multiple orders of magnitude including scales observed in electric potentials and magnetic fields on the scalp, as well as in blood flow signals [8].

Furthermore, the anatomy of the network has an important role in the dynamics. In fact, the topological structure during resting-state is characterized by a combination of high clustering and short path length, typical of small-world networks, which facilitates the information flow and reduces the wiring costs. Moreover, an healthy brain shows a hierarchical modular structure, with sub-networks within networks. As already underlined by other authors, the resting-state is characterized by metastable patterns, involved in periods of synchronization and periods of totally desynchronization. This idea encourages researchers to find methods for studying the interplay between spatial and temporal dimensions during the spontaneous activity. More interestingly in this sense, this pattern formation in FC appears to be correlated with the modularity of the structural connectivity network [16].

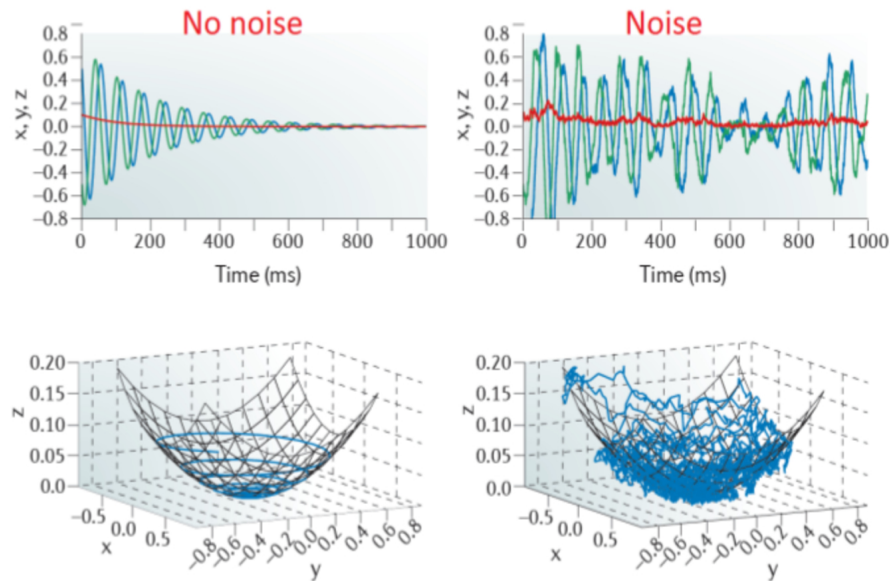


FIGURE 6.7: In this figure are shown the time series (upper part) and the phase plane(lower part) of a three dimensional system with an equilibrium point in order to illustrate the stochastic mechanism that leads to the resting state oscillations. In the absence of noise (left) the system approach to the stable attractor by spiraling down a paraboloid; the corresponding time series of two of the three system variables display a damped oscillation (in green and blue), the third one (in red) relaxes to zero in a non-oscillatory way. In the presence of noise (right)the system explores the neighbourhood of the equilibrium point. Each excursion further away from the equilibrium is followed by an oscillatory return along the paraboloid. This behaviour is revealed in the time series with intermittent, fast neurophysiological oscillations [8].

Besides, in [3] was simulated nonlinear neuronal dynamics on a network that captures the large-scale interregional connections of macaque neocortex. Applying information theoretic measures to identify functional networks, the authors found structure–function relations at multiple temporal scales. So there is not a perfect correspondence between functional activity and underlying connectivity. Functional networks recovered from long windows of neural activity (minutes) largely overlap with the underlying structural network. As a result, hubs in these long-run functional networks correspond to structural hubs. In contrast, significant fluctuations in functional topology are observed across the sequence of networks recovered from consecutive shorter (seconds) time windows. In conclusion FC, when estimated over long time series (called stationary FC), breaks down into a variety of correlation patterns that can be observed only if the estimate is done over short time windows [1], used a technique illustrated in Fig 6.8. Since the correlation over long time series leads, for the definition of the Pearson correlation, to a loss of information about the dynamics evolution of the system, the stationary functional connectivity is mainly related to the underlying anatomy. On the other hand, once FC is estimated over short time windows, it mostly reflects recurrent transitory patterns that aggregate when the FC estimate is done on a whole session.

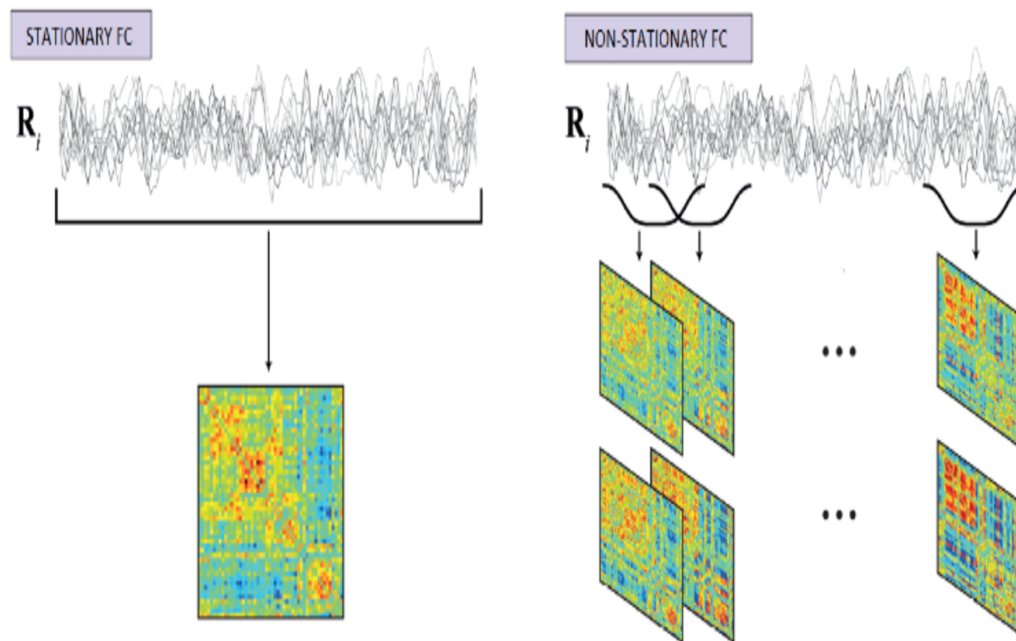


FIGURE 6.8: Schematic representation of sliding windows analysis [1].

It is known that time delays give rise to complex spatiotemporal patterns, oscillations, multistability, and chaos. A common characteristic of the present and previous models is that the optimal operating point for explaining the emergence of RSN is always near a critical point (see Fig.6.9). In other words, the type of local dynamics is relevant for determining the working point that generates resting FC. Nevertheless, in all models, the underlying anatomical structure shapes indeed in the same way as the dynamical landscape that is explored by the noisy fluctuations at its critical working point. This is the reason why, with more or less detail, all these models could explain the spatial functional correlations, which defines the different RSNs. At the edge of the critical instability of any model, the spatial correlations of the noisy excursions are mainly shaped by structure. Critical dynamics are functionally relevant. Indeed, working at the edge of a critical point allows the system to rapidly compute a specific brain function by representing it in an attractor. This may be a fundamental reason why RSNs reflect cognitive functions and why RSNs are so interesting for basic and clinical neuroscience [14].

The neural criticality hypothesis is motivated by the relationship between criticality and optimal computational properties. The hypothesis is supported by experiments that observed hallmarks of criticality for a wide range of animals from leech to humans, over several states of consciousness, and on many different experimental scales from recordings of few neurons up to the whole brain. However, the experimental evidence is still controversial and more studies are needed to resolve major open questions and rule out alternative explanations for the observed phenomena. Based on the presently available works, we judge self-organized criticality as preferable over alternative explanations because it provides an evolutionarily-motivated explanation for several otherwise disconnected observations. In addition to experiments, the criticality hypothesis is supported by models which demonstrate that the self-organization to critical states in the brain is feasible and plausible. The neural

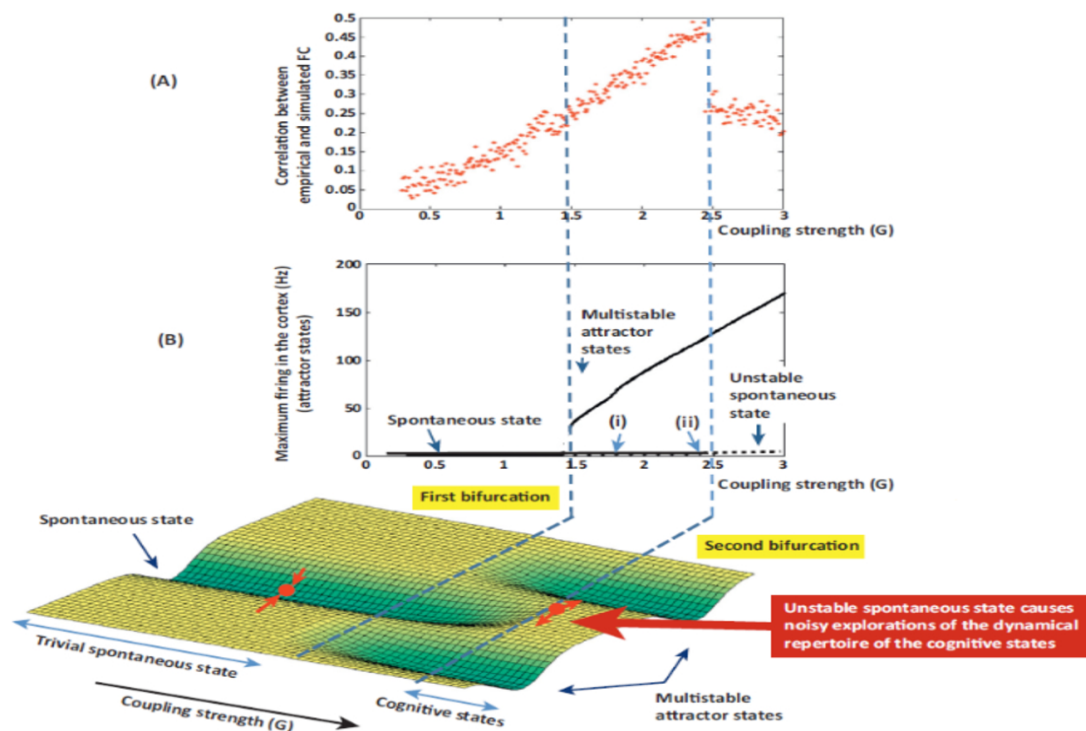


FIGURE 6.9: A) Correlation between the empirical and the simulated functional connectivity with the reduced model is plotted as function of the coupling strength. B) The maximum firing rates activity in function of the coupling strength is shown; in the graph the three different regimes can be observed [15].

criticality hypothesis states that the brain may be poised in a critical state at a boundary between different types of dynamics. Theoretical and experimental studies show that critical systems often exhibit optimal computational properties, suggesting the possibility that criticality has been evolutionarily selected as a useful trait for our nervous system [18].

6.3 Clinical Applications

Most, if not all, physiological and psychiatric diseases have disrupted large-scale functional and/or structural properties. Whether they are the cause or consequence of the disease is unclear, but it was observed that, in these case, brain neural populations exhibit significant changes in dynamic properties; such fact may underlie many of the observed dysfunctions. Quantification of disrupted dynamics in neural populations may lead to a better understanding of the disorder, more targeted drug treatment, and eventually, diagnostic or prognostic indicators. As analysed in the paper [2], there is a relationship between resting state network and mental disorder; the disorders where this link is most evident are autism, schizophrenia and Alzheimer's disease. Others for which hypotheses on the role of DMN have been advanced include depression, obsessional disorders, attention disorders and post-traumatic stress disorder. Moreover, resting state networks take time to emerge in human beings, as it appears from experiments: it is not present in infant and start

being shaped during childhood; changes could be observed in development and aging.

As it concern the concept of criticality, this hypothesis is intriguing because it opens new perspectives in several areas. First, deviations from criticality could be symptomatic of diseases of the central nervous system. Understanding self-organized criticality in the brain could thus lead to new diagnostic tools, and possibly treatments. Second, connections are presently emerging which suggest that understanding criticality in the brain could provide important insights into other phenomena including sleep, learning, the root-causes of certain diseases, and a deeper understanding of information processing [18].

Embracing this perspective, we explore the consequences of network manipulations to understand some of the brain's dysfunctions, as well as network effects that offer new insights into routes towards therapy, recovery and brain repair. These collective insights will be at the core of the new computational environment, the Virtual Brain, which will allow flexible incorporation of empirical data constraining the brain models to integrate, unify and predict network responses to incipient pathological processes. Dynamically comparing scanner results from the real and virtual brain and across imaging modalities paints a bright vision of revolutionary applications as well as a clear pathway to constant future enhancements. For example the brain of a real patient can be scanned and subsequently will be modeled with The Virtual Brain by uploading the scanner results or vice versa; the virtualized brain can be scanned and the readings compared back to the patient's in order to confirm the desired accuracy of the model. In addition new modeling/network hypotheses can be applied to The Virtual Brain and realistically tested through virtual scans and comparison with experimental data. One could even imagine "browsing" through a shelf of different virtual brains until the best match for preset experimental data is found. The combination with the important feedback-loop of virtual therapy proposals and their subsequent experimental validation leads toward a compelling vision: patients suffering from a brain-related disease/injury will be thoroughly scanned, collecting individual EEG, MEG and BOLD data. Complemented with a detailed demographic, genetic and physiological anamnesis, the doctor uploads this data to The Virtual Brain. Evaluating the bespoke simulation, the doctor will be able to judge the patient's brain responses to different therapy approaches - all safely within a virtual framework.

Chapter 7

Conclusion

An interesting interpretation of the resting state network is the one proposed by Deco, Jirsa and McIntosh 2011 [5]; they link brain dynamics at rest to a constant inner state of exploration during which the brain makes prediction about the likely configuration for a given impending input. They explained this concept with an effective metaphor in which they compared the brain at rest to a tennis player waiting for the service of his adversary; during the waiting the player is not static but continues to move with small lateral jumps to be able to react more effectively to the incoming service. The inner brain state exploration is driven by physiological characteristics of the brain such noise, delays in conductions, anatomical connections and intrinsic dynamics. Certainly, there are still many issues that call for further investigations. First of all the accurate definition of the relationship between the anatomical structure and the functional one remains not fully understood, in addition to the connection between the resting-state dynamics and the task-related brain activity. Our future aim reflects the interest in developing a mathematical setting in order to deal not only with normal behaviours but with pathological dynamics as well. In such a perspective, the synthetic control of a possible therapy, flanked to a biological and medical support, could realize a novel perspective for clinical applications.

Furthermore, survival remains the perhaps most important problem faced by brains and a key challenge is how to segregate and integrate relevant information over different time scales when faced with hostile, often constantly changing environments. Reconciling different speeds of information processing, from fast to slow, is especially important, and could be key to the relative evolutionary success of mammals whose sophisticated brains are able to combine prior information from past memories with current stimuli to predict the future and to adapt behaviour accordingly [4]. This was recognized well over a century ago by William James (see citation at the begin of the thesis), generally acknowledged as one of the fathers of modern cognitive psychology. Speaking of this problem using the apt metaphor of the stream of consciousness, James noted that there is a different pace to its parts, comparing it to the life of a bird whose journey consists of an “alternation of flights and perchings”. In the language of today’s dynamical systems, the flights are akin to fast, segregative tendencies and the perchings to slower, integrative tendencies of the dynamic brain in action.

Bibliography

- [1] Allen et al. "Tracking Whole-Brain Connectivity Dynamics in the Resting State". In: *Cerebral Cortex* (2014).
- [2] Buckner et al. "The brain's default network: anatomy, function, and relevance to disease". In: *Ann N Y Acad Sci.* (2008).
- [3] C. J. Honey et al. "Network structure of cerebral cortex shapes functional connectivity on multiple time scales". In: *PNAS* (2007).
- [4] Deco et al. "The dynamics of resting fluctuations in the brain: metastability and its dynamical cortical core". In: *Nature-Scientific Reports* (2017).
- [5] Deco G. et al. "Emerging concepts for the dynamical organization of resting-state activity in the brain". In: *Nature Reviews Neuroscience* (2011).
- [6] Deco G. et al. "Key role of coupling, delay, and noise in resting brain fluctuations". In: *PNAS* (2009).
- [7] Faisal et al. "Noise in the nervous system". In: *Nat Rev Neurosci.* (2009).
- [8] Ghosh et al. "Noise during Rest Enables the Exploration of the Brain's Dynamic Repertoire". In: *PLoS Computational Biology* (2008).
- [9] Kandel E. et al. "Principles of Neural Science". In: (2000). Ed. by McGraw-Hill Medical.
- [10] Knock et al. "The effects of physiologically plausible connectivity structure on local and global dynamics in large scale brain models". In: *Journal of Neuroscience Methods* (2009).
- [11] P. Sanz Leon et al. "The Virtual Brain: a simulator of primate brain network dynamics". In: *Frontiers in Neuroinformatics* (2013).
- [12] A.L.Hodgkin and A.F. Huxley. "a quantitative description of membrane current and its application to conduction and excitation in nerve". In: *J. Physiol.* (1952).
- [13] Snyder A.Z. and Raichle M.E. "A brief history of the resting state: Washington University perspective". In: *The NeuroImage* (2012).
- [14] Ponce-Alvarez et al. Deco. "Resting-State Functional Connectivity Emerges from Structurally and Dynamically Shaped Slow Linear Fluctuations". In: *J.Neurosci.* (2013).
- [15] Jirsa V. K. Deco G. and McIntosh A. R. "Resting brains never rest: computational insights into potential cognitive architectures". In: *Trends in Neurosciences* (2013).
- [16] C. Favaretto and A. Cenedese. "On brain modeling in resting-state as a network of coupled oscillators". In: *Conference on Decision and Control* (2016).
- [17] Deco G. and Jirsa V. K. "Ongoing cortical activity at rest: criticality, multistability and ghost attractors". In: *Journal of Neuroscience* (2012).

- [18] J. Hesse and T. Gross. "Self-organized criticality as a fundamental property of neural systems". In: *Frontiers in Systems Neuroscience* (2014).
- [19] Breakspear M. and Jirsa V. K. "Neural Dynamics and Brain Connectivity". In: (2007). Ed. by Springer.
- [20] Izhikevich E. M. "Dynamical Systems in Neuroscience: The Geometry of Excitability and Bursting". In: (2005). Ed. by MIT press.
- [21] Boccarda N. "Modelling Complex Systems". In: (2010). Ed. by Springer-Verlag New York.
- [22] Sporns O. and Tononi G. "Structural Determinants of Functional Brain Dynamics". In: (2007). Ed. by Springer.
- [23] FitzHugh R. "Impulses and physiological states in theoretical models of nerve membrane". In: *Biophysical Journal* (1961).
- [24] Stefanescu and Jirsa. "A Low Dimensional Description of Globally Coupled Heterogeneous Neural Networks of Excitatory and Inhibitory Neurons". In: *PLoS Computational Biology* (2008).
- [25] Gerstner W. and Kistler W. M. "Spiking Neuron Models Single Neurons, Populations, Plasticity". In: (2002). Ed. by Cambridge University Press.
- [26] H. R. Wilson and J. D. Cowan. "excitatory and inhibitory interactions in localized populations of model neurons". In: *Biophysical Journal* (1972).